The chemistry and saturation states of subsurface fluids during the in situ mineralisation of CO_2 and H_2S at the CarbFix site in SW-Iceland

Sandra Ó. Snæbjörnsdóttir

Institute of Earth Sciences

University of Iceland

Askja

Sturlugata 7

101 Reykjavík, Iceland

tel. 354-525-5414

fax. 354-525-4499

sos22@hi.is

The chemistry and saturation states of subsurface fluids during the *in situ* mineralisation of CO$_2$ and H$_2$S at the CarbFix site in SW-Iceland

Sandra Ó. Snæbjörnsdóttir[1], Eric H. Oelkers[1,2,3], Kiflom Mesfin[1], Edda Sif Aradóttir[4], Knud Dideriksen[5], Ingvi Gunnarsson[4], Einar Gunnlaugsson[4], Juerg M. Matter[6,7], Martin Stute[7], Sigurdur R. Gislason[1]

[1]*Institute of Earth Science, University of Iceland, Iceland*
[2]*CNRS/UMR 5563, Université Paul Sabatier, France*
[3]*Earth Science, University College London, UK*
[4]*Reykjavik Energy, Iceland*
[5]*Nano-Science Center, Department of Chemistry, University of Copenhagen, Denmark*
[6]*Ocean and Earth Science, University of Southampton, UK*
[7]*Lamont-Doherty Earth Observatory, Columbia University, USA*

Abstract

In situ carbonation of basaltic rocks could provide a long-term carbon storage solution, which is essential for the success and public acceptance of carbon storage. To demonstrate the viability of this carbon storage solution, 175 tonnes of pure CO$_2$ and 73 tonnes of a 75% CO$_2$-24% H$_2$S-1% H$_2$-gas mixture were sequentially injected into basaltic rocks at the CarbFix site at Hellisheidi, SW-Iceland from January to August 2102. This paper reports the chemistry and saturation states with respect to potential secondary minerals of sub-surface fluids sampled prior to, during, and after the injections. All gases were dissolved in water during their injection into permeable basalts located at 500-800 m depth with temperatures ranging from 20 to 50°C. A pH decrease and dissolved inorganic carbon (DIC) increase was observed in the first monitoring well, HN-04, about two weeks after each injection began. At storage reservoir target depth, this diverted monitoring well is located ~125 m downstream from the injection well. A significant increase in H$_2$S concentration, however, was not observed after the second injection. Sampled fluids from the HN-04 well show a rapid increase in Ca, Mg, and Fe concentration during the injections with

31   a gradual decline in the following months. Calculations indicate that the sampled fluids are

32   saturated with respect to siderite about four weeks after the injections began, and these fluids

33   attained calcite saturation about three months after each injection. Pyrite is supersaturated prior

34   to and during the mixed gas injection and in the following months. In July 2013, the HN-04 fluid

35   sampling pump broke down due to calcite precipitation, verifying the carbonation of the injected

36   CO_2. Mass balance calculations, based on the recovery of non-reactive tracers co-injected into

37   the subsurface together with the acid-gases, confirm that more than 95% of the CO_2 injected into

38   the subsurface was mineralised within a year, and essentially all of the injected H_2S was

39   mineralised within four months of its injection. These results demonstrate the viability of the *in*

40   *situ* mineralisation of these gases in basaltic rocks as a long-term and safe storage solution for

41   CO_2 and H_2S.

42

43   **Introduction**

44   Attenuating the current increasing atmospheric CO_2 concentration is one of the greatest

45   challenges of this century (e.g. Broecker, 2007; Broecker and Kunzig, 2008; Global CCS Institute,

46   2015; Hoffert et al., 2002; International Energy Agency, 2015 ; IPCC, 2005, 2014; Lackner, 2003;

47   Oelkers and Schott, 2005; Oelkers and Cole, 2008; Pacala and Socolow, 2004). One potential

48   solution to this challenge is carbon capture and storage (CCS). A critical step in CCS is identifying

49   locations and methods for secure subsurface CO_2 storage.

50

51   This paper follows two previous reports on the CarbFix injection, 1) a detailed description

52   of the injection method and data from the injection well was presented by Sigfússon et al. (2015)

53   and 2) the monitoring of tracers, carbon and pH in the first monitoring well downstream from the

54   injection well was reported by Matter et al. (2016). The CarbFix project is focussed on CO_2 and

55   H_2S injected into basaltic rocks. Carbon storage in basaltic rocks offers several advantages, due to

56   their ability to promote permanent CO_2 storage by mineralisation and due to their large potential

57   storage volume (Gislason and Oelkers, 2014; Goldberg and Slagle, 2009; Goldberg et al., 2010;

58   McGrail et al., 2006; Snæbjörnsdóttir et al., 2014). As such, a large number of past studies have

59   focussed on developing the technology to safely store CO_2 in basaltic rocks (Assayag et al., 2009;

60   Bacon et al., 2014; Flaathen et al., 2009; Galeczka et al., 2014; Goldberg et al., 2013; Goldberg et

61   al., 2008; Gudbrandsson et al., 2011; Gysi and Stefánsson, 2012a; Matter et al., 2007; McGrail et

62 al., 2012; McGrail et al., 2006; McGrail et al., 2011; Rogers et al., 2006; Rosenbauer et al., 2012;

63 Sigfusson et al., 2015; Stockmann et al., 2011; Van Pham et al., 2012). Basaltic rocks are rich in

64 divalent cations such as Ca^{2+}, Mg^{2+}, and Fe^{2+}. Acidic gas-charged water accelerates the release of

65 these metals, promoting the formation of carbonate minerals such as calcite, magnesite, and

66 siderite (Gislason et al., 2014; Gislason and Oelkers, 2014; Olsson et al., 2014; Gislason et al.,

67 2010; Gunnarsson et al., 2011; Oelkers et al., 2008; Stefánsson et al., 2011). About 10% of the

68 continents and most of the oceanic floor are comprised of basaltic rocks, including the mid-oceanic

69 ridges. The largest basaltic storage potential lies offshore; theoretically all CO_2 from the burning of

70 fossil fuel carbon (~5000 GtC; Archer, 2005) could be stored by mineral carbonation along the

71 mid-ocean ridges (Snæbjörnsdóttir et al., 2014). The flanks of the ridges contain highly fractured

72 and permeable basaltic layers (Fisher, 1998) with a pervasive circulation of about 1,000 Gt

73 seawater/yr (Harris and Chapman, 2004). The potential for using these systems for carbon storage

74 is confirmed by the results of Wolff-Boenisch et al. (2011), who demonstrated the rapid

75 dissolution basaltic rocks in CO_2 charged seawater.

76

77   About 90% of Icelandic bedrock is basaltic (Hjartarson and Sæmundsson, 2014). In total,

78 Iceland produced 1.6 $MtCO_2$ by industrial processes in 2012 and about 0.2 $MtCO_2$ by geothermal

79 energy production (Wöll et al., 2014). Iceland is the largest (103,000 km^2) part of the mid-ocean

80 ridge systems exposed above sea level. Iceland, therefore, provides an excellent opportunity to

81 explore the feasibility of mineral storage of CO_2 and gas mixtures in basaltic rocks at the oceanic

82 ridges since drilling and detailed monitoring of injected gas and water by reactive and non-reactive

83 tracers is much less costly onshore than offshore.

84

85   The potential advantages in storing carbon by the *in situ* carbonation of Icelandic basalts

86 motivated creation of the CarbFix project, which was designed to inject CO_2 into subsurface

87 adjacent to the Hellisheidi geothermal power plant. Extensive research was carried out prior to the

88 injection of acid gases at the CarbFix site. Gislason et al. (2010) described the thermodynamics

89 and kinetic basis for carbon storage at this site. Alfredsson et al., (2013) characterised the geology,

90 and rock and water chemistry of the CarbFix site. Wiese et al. (2008) determined the amount and

91 spatial distribution of naturally mineralised CO_2 within the Icelandic geothermal systems. The

92 dissolution and precipitation rates of the subsurface rocks at the site were investigated in mixed

93 flow reactors (e.g. Gudbrandsson et al., 2011; Gysi and Stefánsson, 2012a; Stockmann et al.,

94 2013), in pressurised plug flow experiments (e.g. Galeczka et al., 2014), by hydrological modelling

95 (Khalilabad et al., 2008), and using reactive transport modelling (Aradóttir et al., 2012).

96

97   The CarbFix project is unique in that it injects CO_2 into basalts as a dissolved aqueous

98 phase. In contrast, most subsurface carbon storage projects have injected CO_2 as a separate phase

99 into large sedimentary basins; this method requires high integrity cap-rocks to keep the injected

100 buoyant gas in the subsurface (Gislason and Oelkers, 2014; Rutqvist et al., 2007). However, there

101 are numerous advantages of injecting CO_2 into the subsurface within an aqueous phase. First,

102 many of the risks associated with buoyancy can be mitigated by dissolving the gases into water

103 during their injection (Gislason et al., 2010; Sigfusson et al., 2015). Once dissolved, the injected

104 gases are no longer buoyant, making it possible to inject CO_2 into fractured rocks, such as basalts

105 along the ocean ridges and on the continents. Furthermore, this injection method may also make it

106 possible to simultaneously store a number of acid gases including SO_2 and H_2S as sulphide

107 minerals such as pyrite and pyrrhotite, lowering substantially gas capture/storage costs (Gislason et

108 al., 2014; Gislason and Oelkers, 2014; WorleyParsons and Schlumberger, 2011).

109

110   Large SO_2 emissions are associated with fossil fuel power production and heavy industry

111 such as metal smelters (Smith et al., 2011). These emissions peaked in 1970-1980 at about 80 Mt

112 per year in the USA and Europe leading to acid rain and Al mobilisation, degrading aquatic and

113 terrestrial ecosystems (Gensemer and Playle, 1999; Gislason and Torssander, 2006). Due to

114 intervening regulations, these emissions have been in decline, and were less than 11 Mt in 2011

115 (European Environment Agency, 2014; United States Environmental Protection Agency, 2015)

116 due, in large part due to SO_2 capture. This SO_2 capture could potentially be combined with CO_2

117 capture in water, and this water-soluble gas mixture injected into reactive rocks for mineral

118 storage.

119

120   Emissions of H_2S are an inevitable consequence of geothermal energy exploitation, pulp

121 and paper production and the use of fossil fuels (e.g.World Health Organization, 2000).

122 Regulations for H_2S emissions have obliged Icelandic geothermal energy producers to reduce their

123 emissions of this gas (Aradóttir et al., 2015; Gunnarsson et al., 2011). One mitigation option is to

124 capture H$_2$S and inject it into the subsurface. This approach has been adopted by an ongoing
125 carbon storage project at Weyburn Canada in connection with enhanced oil recovery, which has
126 been co-injecting supercritical CO$_2$ and H$_2$S into subsurface sedimentary rocks (Bachu and Gunter,
127 2005). The behaviour of co-injecting H$_2$S has not been studied to the same extent as injection of
128 pure CO$_2$. Some work has, however, been done in terms of geochemical modelling and laboratory
129 experiments (e.g. Bacon et al., 2014; Gudbrandsson and Stefánsson, 2014; Gunnarsson et al.,
130 2011; Stefánsson et al., 2011; Knauss et al., 2005). One goal of the CarbFix project is to assess the
131 feasibility of co-injecting dissolved H$_2$S and CO$_2$ into basalts which can provide a cost effective
132 storage solution for both of these gases.

133

134   This paper reports on our further efforts to develop the technology to store CO$_2$ through the
135 *in situ* carbonation of basaltic rocks at the CarbFix storage site in southwest Iceland. Two field
136 injections were carried out at this storage site. In January to March 2012, 175 tonnes of pure CO$_2$
137 were injected into the CarbFix site. In June to August 2012, 73 tonnes of a gas mixture from the
138 Hellisheidi geothermal power plant were injected, consisting of 75 mol% CO$_2$, 24 mol% H$_2$S and 1
139 mol% H$_2$. In each case, the gases were dissolved into formation water during their injection,
140 releasing a single aqueous fluid into the storage formation. Here we report the compositions and
141 saturation states of fluid samples collected from a diverted monitoring well located 125 m in the
142 down-flow direction of the injection well at target storage reservoir depth, before, during, and after
143 the CO$_2$ and CO$_2$-H$_2$S injections, and use these results to better understand the fate of these
144 injected gases in the subsurface.

145

146

147 **Methods**

148 **Description of the CarbFix site**

149   The CarbFix injection site is located in SW-Iceland, about 30 km east of Reykjavík. The
150 site is ~260 m above sea level and located 3 km SW of the Hellisheidi geothermal power plant
151 (Fig. 1), which is owned and operated by Reykjavik Energy. During 2015, the power plant
152 generated 303 MW of electricity and 133 MW of thermal energy using hot water and steam from
153 a high temperature reservoir located at 800-3000 m depth E and NE of the power plant. The

154 power plant annually produces 40,000 tonnes CO_2 and 12,000 tonnes H_2S. These gases are of

155 magmatic origin produced as a by-product of the geothermal energy production.

156

157   Acidic gases injected at the CarbFix site were dissolved into water collected from HN-01,

158 a well located about 1 km west of the 2001 m deep HN-02 injection well (Fig. 1). Well HN-01 is

159 1306 m deep; water collected from this well was transported via pipeline to HN-02 where the

160 HN-01 water was injected through a pipe as described in detail by Sigfusson et al. (2015). The

161 injected gas was released into the down flowing water via a sparger at a depth of 340 m. The gas

162 dissolved in the water as it was carried down a mixing pipe to a depth of 540 m, where the

163 hydrostatic pressure is above 40 bars, ensuring complete dissolution of the CO_2 before it was

164 released into the subsurface rocks (Aradóttir et al., 2012; Gislason et al., 2010; Sigfusson et al.,

165 2015).

166

167   The geology of the CarbFix site was described in detail by Alfredsson et al. (2013). The

168 subsurface rocks at the injection site are primarily olivine tholeiite basalts, consisting of post-

169 glacial lava flows and glassy hyaloclastite formations, formed beneath the ice-sheet during

170 glaciations (Fig. 1). The bedrock down to about 200-300 m depth consists of relatively unaltered

171 olivine tholeiite lava flows that host an oxygen-rich groundwater system with a static water table

172 at about 100 m depth. Below the lava flows lies a 200 m thick, slightly altered hyaloclastite that

173 separates the near surface water system from a deeper system, which is oxygen depleted. The site

174 follows an approximately linear temperature gradient of 80°C/km. The target injection formation

175 consists of a series of altered lava flows from about 400 m to 800 m depth overlain by the low

176 permeability hyaloclastites (Alfredsson et al., 2013; Helgadóttir, 2011). The lateral and vertical

177 intrinsic permeabilities of the storage formation were estimated to be 300 and 1700 x 10^{-15} m^2,

178 respectively, having an effective matrix porosity of 8.5% and a 25 m/year estimated regional

179 groundwater flow velocity (Aradóttir et al., 2012). The most abundant alteration minerals from

180 200 m to 1000 m depth are smectites, calcite, and Ca- and Na-rich zeolites (Alfredsson et al.,

181 2013; Helgadóttir, 2011).

182

183   The injection site is equipped with eight monitoring wells ranging from 50 to 1300 m

184 depth. Six of the eight wells are located downstream from the HN-02 injection well. Four of the

185 wells penetrate the groundwater system in the topmost 200-300 m and four are drilled down
186 through the target storage formation. These deeper wells are cased down to 400 m depth and
187 serve as monitoring wells of the deeper system. All monitoring wells were sampled during the
188 experiment, but evidence of tracers from the injections has only been found, to date, in samples
189 collected from well HN-04, which is the closest to the injection well as shown in Figure 1. Well
190 HN-04 is located about 10 m west of HN-02 at the surface, but it is diverted in the subsurface
191 such that the distance between the wells is 125 m at 520 m depth, where the target carbon storage
192 aquifer is located (Alfredsson et al., 2013; Aradóttir et al., 2012). Field injections at the CarbFix
193 site were performed from 2008 to 2012. Tracer tests were conducted both under natural and
194 forced flow conditions from 2008 to 2011 to define the system hydrology and for scaling
195 reactive transport models (Aradóttir et al., 2012; Gislason et al., 2010; Khalilabad et al., 2008;
196 Matter et al., 2011).

197

198 **Acid Gas Injections at the CarbFix site**

199 The injection of acid gases at the CarbFix site was performed in two phases during 2012
200 (Table 1):

201

202 **Phase I** began in late January 2012 with the injection of 175 tonnes of pure CO_2. The CO_2 was
203 stored in a 30 m^3 reservoir tank pressurised at 26-28 bars and co-injected with water collected
204 from well HN-01 into well HN-02, as described by Sigfusson et al. (2015). The predicted *in situ*
205 pH and DIC concentrations of the injected fluid during Phase I were 3.85 and 0.823 mol kg^{-1}
206 respectively, based on the mass flow rates of water and gas into the injection well, chemical
207 speciation calculations (Parkhurst and Appelo, 2013), and direct measurement (Sigfusson et al.,
208 2015). The chemical tracers listed in Table 1 were co-dissolved into the injected water as
209 described by Sigfusson et al. (2015) to aid in determining the fate of the dissolved CO_2 as
210 described by Matter et al. (2016). The Phase I injection ran continuously until it was terminated
211 on the 9th of March 2012.

212

213 **Phase II** began in mid-June 2012 with the injection of 73 tonnes of a gas mixture containing 75
214 mol% CO_2, 24 mol% H_2S, and 1 mol% H_2 originating from the Hellisheidi power plant. The gas
215 mixture was obtained by diverting power plant emissions to a gas abatement plant, where it was

216 separated into water soluble gases (CO_2, H_2S), and less soluble gases (N_2, CH_4, H_2, Ar). The

217 power plant emission gas contained about 20% H_2; a small fraction of this dissolves in the water

218 along with the CO_2 and H_2S according to the solubility and partial pressure of the gases.

219 Subsequently the soluble gas mixture was co-injected into the surface with HN-01 water. The

220 predicted *in situ* pH, DIC, H_2S, and H_2 concentrations of the injected water during the Phase II,

221 based on the mass flow rates of water and gas into the injection well and chemical speciation

222 calculations performed using PHREEQC (Parkhurst and Appelo, 2013) were 4.03, 0.43 mol kg^{-1},

223 0.14 mol kg^{-1} and less than 0.01 mol kg^{-1}, respectively. The chemical tracers listed in Table 1

224 were co-dissolved into the injected water as for the pure CO_2 injection to monitor subsurface

225 reactivity. The gas mixture injection rate was less stable than that of the pure CO_2 injection and

226 was stopped several times due to injection problems. The injection was terminated on the 1st of

227 August 2012.

228

Analytical methods

230   Sampling of the fluids from the HN-04 first monitoring well began in 2008. Water

231 samples for chemical analysis were collected several times prior to the Phase I injection in

232 January 2012 (Alfredsson et al., 2013). During the injections and until mid-September 2012 this

233 well was sampled twice weekly. Weekly sampling continued until mid-July 2013 with few

234 exceptions.

235

236   Water was pumped from the monitoring well at the rate of 3.5 m^3/h throughout this study,

237 to maintain a constant head from the injection to the monitoring well. The pump used was a

238 163 cm long, submersible Grundfos model SP3A-60 made of stainless steel, located at 303 m

239 depth and ~200 m below the water table. This pump was connected to a 53 mm diameter steel

240 pipe to the surface where the effluent was deposed via a service pipe extending east of the

241 injection site and eventually re-injected into a deep geothermal system.

242

243   Fluid samples were collected via a 10 m long, 10 mm diameter stainless steel pipe

244 connected to the 53 mm diameter monitoring well lining pipe extending down to the pump. The

245 10 mm sample pipe was connected directly to a sampling valve inside an on-site field laboratory.

246 After flushing the sampling pipe, the sampled waters were immediately filtered through 0.2 μm

247   Millipore cellulose acetate membranes using silicon tubing and a 140 mm Sartorius®

248   polypropylene filter holder. All air in the filtration system was expelled through a valve prior to

249   sampling and at least 3 L of water was pumped through the system before the samples were

250   collected in distinct bottles depending on the subsequent chemical analysis. Amber glass bottles

251   were used to collect samples for pH and alkalinity. Acid washed high density polyethylene

252   bottles were used to collect samples for cations and trace metals. These samples were acidified

253   using Suprapur® HNO_3, 1% (v/v). Acid washed low density polypropylene bottles were used to

254   collect samples for Fe-species measurement. These samples were acidified with Suprapur® HCl,

255   1% (v/v) immediately after collection. Low density polypropylene bottles were used for

256   collecting samples for anion concentration measurements. Acid washed polycarbonate bottles

257   were used to collect samples for dissolved organic carbon (DOC). These samples were acidified

258   with 1.2 M concentrated HCl 2% (v/v). All sample bottles were rinsed three times by half filling

259   them with the filtrated water and then emptying them prior to sample collection.

260

261   Temperature and conductivity were measured at the sampling site using a Eutech

262   Instruments Oakalon 2-cell Conductivity meter. The *in situ* temperature of the sampled fluid was

263   determined using down-hole temperature logging at the depth of the main feed-point of well HN-

264   04, at about 420 m depth (Alfredsson et al., 2013; Thorarinsson et al., 2006). The pH was

265   determined on site with a Eutech InstrumentsTM CyberScan pH 110 electrode and again in the

266   laboratory a few hours after sampling with a Cole Parmer combined glass electrode together with

267   an Orion pH meter. The uncertainty of the analyses is estimated to be ±0.02. The pH was then re-

268   calculated at *in situ* conditions using PHREEQC (Parkhurst and Appelo, 2013). Alkalinity was

269   measured in the laboratory by alkalinity titration using the Gran function to determine the end

270   point of the titration (Stumm and Morgan, 1996). Total dissolved inorganic carbon (DIC) was

271   calculated with PHREEQC (Parkhurst and Appelo, 2013) using measured pH, alkalinity,

272   temperature and total dissolved elements concentrations. The uncertainties of the DIC

273   calculations are estimated to be within 10%.

274

275   Dissolved oxygen was fixed on site and later determined by Winkler titration. This

276   method has a precision of 1 μmol/L O_2 (0.03 ppm) for the 50 ml sample bottles, but there is a

277   risk of atmospheric contamination for samples containing no or little oxygen. Such is the case for

278   the samples collected from HN-04, which are oxygen depleted. The O_2 concentrations of the
279   sampled fluids ranged from 2-24 µmol/L. The difference between the O_2 concentration in the
280   samples and the reagents was determined using the method described by Arnórsson (2000). The
281   results show that the oxygen measured in the samples is mostly derived from the reagents. Some
282   oxygen contamination during sampling was also inevitable.

283

284   Dissolved hydrogen sulphide was measured by titration on site using mercury and
285   dithizone as an indicator (Arnórsson et al., 2000). The sensitivity of this method is about 0.29
286   µmol/L H_2S (about 0.01 ppm) when using a 50 ml sample aliquot.

287

288   The major elements Si, Ca, K, Mg, Na, and S and the trace metals Fe and Al were
289   analysed using a Spectro Ciros Vision Inductively Coupled Plasma Optical Emission
290   Spectrometer (ICP-OES) using an in-house multi-elements standard checked against the SPEX
291   Certified Reference standard at the University of Iceland. The samples were analysed again using
292   a Agilent 725 ICP-OES for major elements and an ELEMENT XR Inductively Coupled Plasma
293   Sector Field Mass Spectrometer (ICP-SFMS) from ThermoScientific for the trace elements Fe
294   and Al at ALS Scandinavia, Luleå, Sweden. Analytical measurements for the major elements had
295   an inter-laboratory reproducibility within 12%. The average difference between corresponding
296   concentration measurements is 3.7% with a standard deviation of 2.3%. Analytical
297   measurements for the trace elements Fe and Al had an inter-laboratory reproducibility within
298   19%. The average difference in corresponding Fe and Al concentration measurements was 4.9%.
299   Dissolved F^-, Cl^-, and SO_4^{-2} concentrations were quantified using a DIONEX, ICS-2000 Ion
300   Chromatograph. The addition of zinc-acetate to the SO_4 sample was not needed for its analysis
301   since the H_2S concentrations were small compared to the SO_4 concentrations as shown below.
302   Concentrations of Fe^{2+} and Fe^{3+} were measured using a DIONEX IC-3000 Ion Chromatograph.
303   Due to ambiguities in the Fe^{3+} measurements, the Fe^{2+} measurements were used along with the
304   Fe_{total} concentrations measured by ICP-SFMS at ALS Scandinavia to calculate Fe^{3+}
305   concentrations. Analysis of dissolved organic carbon (DOC) was carried out at Umeå Marine
306   Science Center in Umeå, Sweden using a Shimadzu TOC-VcPH total organic carbon analyser.

307

308   The precipitates collected from the pump recovered from the HN-04 monitoring well
309   were analysed by X-ray Powder Diffraction (XRD) at ISOR, Iceland for phase identification.
310   The samples were measured using a Bruker AXS D8 Focus X-ray diffractometer with Cu kα
311   radiation at 1.54Å wavelength, set at 40 kV and 40 mA using 1° divergence and receiving slits.
312   The chemical composition of the precipitates was also analysed by ALS, Scandinavia. The
313   precipitates were digested in HNO_3 and HCl with a trace of HF in a microwave oven. The
314   resulting fluids were then analysed using both ICP-OES and High Resolution Inductively
315   Coupled Plasma Mass Spectrometry (HR-ICP-MS). Detection limits were in the range of 0.01
316   ppm for trace elements to single ppm for major elements, and uncertainties for concentrations 10
317   times these detection limits are within 10% of the reported value.

318

319   Precipitates from samples collected from an air-lift of the HN-02 injection well in June
320   2013, were analysed for phase identification by XRD at the University of Copenhagen, Denmark
321   with a Bruker D8 Discover equipped with a Co tube. 1L slurries collected from the air-lift were
322   sealed immediately after sampling, transported to Denmark, where they were kept in an
323   anaerobic chamber prior to analysis to minimise oxidation. Within the chamber, the samples
324   were centrifuged, dried, crushed and mounted on low-background sample holders that were then
325   covered with X-ray transparent cups to minimise oxidation during measurements.

326

327   **Mass balance calculations**

328   The fate of injected gases in this study are evaluated with the aid of mass balance
329   calculations based on the injected non-reactive tracers SF_6 and SF_5CF_3 (Assayag et al., 2009;
330   Matter et al., 2007; Matter et al., 2016). All collected water samples consist of a mixture from
331   three sources; the original groundwater, that injected during Phase 1 and that injected during
332   Phase 2. In the absence of reactions that remove or add material to the mixed fluid, mass balance
333   requires that the concentration of chemical component i in the monitoring well samples (c_i) to be

334

335    $$c_i = c_{i,GW}X_{GW} + c_{i,1}X_{i,1} + c_{i,2}X_2 \qquad (1)$$

336

337   where $c_{i,GW}$, $c_{i,1}$, and $c_{i,2}$ refers to the concentration of the ith chemical component in the original

338   groundwater, the Phase 1 injection and the Phase 2 injection, respectively, whereas and X_{GW}, X_1,

339   and X_2 designate the fraction of the these three fluid sources in each monitoring sample.

340

341   The fraction of each water source in each monitoring sample was determined from the

342   measured concentrations of the two non-reactive tracers, SF_6 and SF_5CF_3 together with the

343   requirement that

344

345      $$X_{GW} + X_1 + X_2 = 1 \qquad\qquad\qquad (2)$$

346

347   Comparison of values based on the assumption of non-reactive mixing, obtained from

348   Eqns. (1) and (2), with those measured in the monitoring wells provides an estimate of the

349   percentage of injected gases fixed by chemical reactions, and the mass of elements added or

350   removed from the fluid by mineral dissolution and precipitation reactions due to the injections.

351   The background concentration of SF_6 in Eqn. 1 ($c_{i,GW}$) was not constant with time since SF_6 had

352   been used in previous hydrological tests. This background concentration was corrected by taking

353   account of the sample sodium fluorescein tracer concentrations; this tracer was co-injected with

354   the SF_6 in the previous tests as described by Matter et al. (2016).

355

356   Sample 12KGM06 (Table 2) of the injected water from well HN-01 was used to constrain

357   the elemental concentrations of the injected fluid, apart from the elements C and S, which were

358   determined by accounting for the concentration of CO_2 and H_2S added to these injected fluids.

359   Sample 12KGM01 (Table A1 in the electronic supplements) collected from well HN-04 before

360   injection was used for representing the ambient groundwater concentrations. Mass balance

361   calculations were performed for the major elements Ca, Mg, Si, Na, K, and Cl, and the trace

362   elements Fe and Al.

363

364 **Geochemical modelling**

365   Modelling of the water chemistry, including the calculation of percent error in charge

366   balance, the *in situ* saturation state of the water with respect to mineral and gas phases, and the

367   effect of CO_2 and CO_2-H_2S-H_2 gas injection on the aqueous chemistry of the subsurface fluids

368   was performed using PHREEQC (Parkhurst and Appelo, 2013). In no case did the charge
369   imbalance exceed 6.1%. The standard PHREEQC database was used in all calculations after
370   including revised thermodynamic data on secondary minerals taken from Gysi and Stefánsson
371   (2011), and pyrrotite and greigite taken from the MINTEQ and the llnl databases, respectively,
372   as described in Alfredsson et al. (2013). Dissolved inorganic carbon (DIC) was calculated for
373   each water sample using measured alkalinity, pH and temperature defined at 35°C at the *in situ*
374   conditions. All saturation indices were calculated assuming the oxygen fugacity was controlled
375   by equilibrium with the H_2S/SO_4^{2-} as a redox couple. For samples having no measured excess
376   H_2S, the H_2S concentration was assumed to be equal to the detection limit of the H_2S titration, as
377   geothermal waters always contain a small fraction of H_2S although below the detection limit.

378

379 Results

380   The compositions of all sampled fluids are shown in Figures 2, 3, and 8, Table 2 and
381   Table A1 in the electronic supplements. An increase in the non-reactive sulphur hexafluoride
382   (SF_6) tracer, indicating the initial arrival of the migrating dissolved CO_2 plume in the HN-04
383   monitoring well, occurred about two weeks after the start of the Phase I injection (Fig. 2a). The
384   concentration of this tracer increased until a maximum 56 days after the Phase 1 injection started
385   (Matter et al., 2016). The SF_6 tracer concentration again increased about 100 days after the
386   injection started, reaching an overall maximum about 13 months after Phase I was started (see
387   Fig 2a; Matter et al., 2016). This is the same pattern observed during the previous tracer test
388   (Khalilabad et al., 2008), indicating that the storage formation consists of relatively homogenous
389   porous media intersected by a low volume and fast flow path that channels about 3% of the
390   tracer flow between wells HN-02 and HN-04. The same pattern was observed for Phase II, with
391   the first arrival of the non-reactive trifluoromethyl sulphur pentafluoride (SF_5CF_3) tracer
392   observed about two weeks after the start of the mixed-gas injection (Fig. 2a), with an initial
393   smaller maximum about 60 days after the injection began (Matter et al., 2016). A further increase
394   in SF_5CF_3 was noted about 150 days after Phase II injection began (Fig. 2a), consistent with the
395   behaviour of SF_6 (Matter et al., 2016). The second SF_5CF_3 concentration maximum was not
396   observed due to a breakdown of the submersible pump in the monitoring well HN-04, resulting
397   in a three month gap in the monitoring data as described below.

398

Fluid pH, carbon, and sulphur

Prior to the injections, the pH of the HN-04 monitoring well samples was 9.5-9.6, the DIC was 1.3-1.4 mmol/L, and the total S concentration was 0.09-0.11 mmol/L (see Fig. 2b-c, Table A1 in the electronic supplements, and Alfredsson et al. (2013)). The measured pH and DIC before, during and after the two injection phases are shown in Figure 2b. The pH of the sampled fluids is extremely sensitive to the injection of dissolved gases. The pH *in situ* (35°C) decreases from 9.6 prior to each injection to approximately 7 near the end the injection then subsequently recovers to a value higher than 9. The decrease starts about two weeks after the start of Phase I, contemporary with the first arrival of the non-reactive tracer. The lowest pH following Phase I was 6.6 and occurred at the same time as the highest DIC value of 4.4 mmol/L, about 50 days after the Phase I injection was started, but ten days before the first reactive tracer maximum. Subsequently, both DIC and pH trended back towards their initial values (Fig. 2b). A similar pattern was observed during Phase II; the pH began to drop about two weeks after the injection was started, with the lowest pH of 7.1 measured at the same time as the highest DIC value of 3.3 mmol/L, about 60 days after the Phase II injection was started and concurrent the first SF_5CF_3 tracer maximum (see Fig 2).

No corresponding increase in DIC was observed during the second and larger SF_6 tracer maximum. This suggests significant mineral storage of the injected carbon; the difference between measured and calculated DIC indicate that >95% of the injected CO_2 was mineralised in less than two years, as previously reported by Matter et al. (2016). The second and larger SF_5CF_3 tracer maximum was not observed due to a pump failure in the HN-04 monitoring well, but an increase was noted in this concentration approximately one year after the start of the Phase II injection, consistent with the increase during the second breakthrough of SF_6. No corresponding increase in DIC was observed. Analysis of dissolved organic carbon (DOC) show continuous decrease in DOC concentrations from the start of Phase I, and throughout the monitoring period, except for a small increase shortly after the termination of the Phase II, from August to September 2012 (Table A1 in the electronic supplements). The measured DIC concentration is more than two orders of magnitude greater than the measured DOC concentration throughout most of the monitoring period after the Phase I injection (Fig. 2b and Table A1 in the electronic supplements).

430

431   The measured sulphur concentrations (SO_4^{-2}, H_2S, and S total) from before, during and

432   after the Phase II injection are shown in Figure 2c and Table A1 in the electronic supplements.

433   The concentrations are close to constant throughout this two year study. The average SO_4^{-2}

434   concentration measured by IC-2000 during the period was 0.10±0.01 mmol/L, with a standard

435   deviation of 0.005. The average total S concentration measured by ICP-OES was 0.10±0.02

436   mmol/L, with standard deviation of 0.003. The H_2S concentrations were, in most cases, close to

437   the 0.3 µmol/L detection limit. The highest H_2S concentration, 1.5 µmol/L, was measured during

438   the Phase II injection. The H_2S sulphur species always comprised less than 1.5% of the total

439   dissolved S measured by the ICP-OES. This suggests an even more rapid mineralisation of the

440   injected H_2S than the injected CO_2; no significant increase in sulphur concentrations was noted

441   during this field injection experiment, indicating that all of the injected sulphur was mineralised

442   before the first reactive tracer maximum of the SF_5CF_3 was observed in the monitoring well HN-

443   04, or within 60 days of the start of the injection.

444

Major and trace elements

446   The release of the divalent cations Ca^{2+}, Mg^{2+}, and Fe^{2+} from the host basalt is essential

447   for the mineralisation of the injected gases. The chemical compositions of the HN-04 monitoring

448   samples demonstrate the rapid increase in Ca, Mg, and Fe concentration during the two injection

449   phases with a gradual decline in the following weeks and months (see Fig. 3a-c). The increases

450   in these concentrations were first observed concurrently with the first appearance of the non-

451   reactive tracers. The Fe^{2+} was not detected in any sample after early April 2013, or about 6

452   weeks after the major part of the injected Phase 1 fluid arrived in well HN-04 and the Fe^{2+}

453   concentrations were close to the detection limit for the two months following the start of the gas

454   mixture injection.

455

456   In contrast, dissolved Si concentrations were close to constant throughout the monitoring

457   period (Fig. 3d). An increase in Na concentration was most prominent at the beginning of the

458   Phase I injection when its concentration increased from 2.1-2.2 mmol/L to about 2.3-2.4 mmol/L

459   (Fig. 3e). Another increase was observed during the Phase II injection to about 2.5 mmol/L. The

460   Na-concentration at the end of the monitoring period was about 2.6-2.7 mmol/L. A similar trend

461   is evident for K, but the increase in its concentration was somewhat lower than that of Na (Fig.

462   3f). The only major difference between the responses of these concentrations to the dissolved gas

463   injections was the presence of a small concentration peak in K during October 2012. The origin

464   of this peak in unclear. The Al concentrations were strongly pH dependent, consistent with its

465   solubility dependence on pH from neutral to basic conditions (e.g. Drever, 1982). As such, a

466   strong correlation was observed between Al concentrations and pH before, during, and after the

467   injections (Fig. 3g). The Cl concentrations were generally constant throughout the monitoring

468   period with a concentration of 2.4 mmol/L (Fig. h).

469

Calcite precipitates

471   In July 2013, about one and a half years after the start of the Phase I injection, the

472   submersible pump in well HN-04 broke down. When the pump was brought to the surface, it was

473   found to be clogged and coated with a green precipitate as shown in Figure 4. No precipitation

474   was observed on the pump prior to the injections. The bulk chemical compositions of the

475   precipitate samples are shown in Table 3. The cation concentration of the precipitates consisted

476   mostly of calcium (>94%) with some iron (<3%), silica (<2%) and magnesium (<1%). The

477   XRD-analysis (Fig. A2 in the electronic supplements) confirmed that calcite was the dominant

478   mineral phase of this precipitate and no other crystalline phases were identified. A ^{14}C analysis

479   of the carbon in the precipitates confirms that they originated from the injected ^{14}C labelled CO_2

480   (Matter et al., 2016).

481

Mineral saturation states of C- and S-bearing minerals

483   The saturation indices (SI) of calcite ($CaCO_3$), magnesite ($MgCO_3$) and siderite ($FeCO_3$),

484   as calculated using PHREEQC, are shown in Figure 5a. Calculations show that calcite was

485   saturated both before and after the Phase I and Phase II injections. This mineral was, however,

486   strongly undersaturated just after these injections concurrent with the drop in monitoring fluid

487   pH below 8, even though the DIC and Ca concentrations were relatively high (Figs. 2a and 3a).

488   Note that calcite was identified by XRD-analysis on drill-cuttings from the area prior to the

489   injections (Alfredsson et al., 2013) and within and on the pump in the monitoring well at the end

490   of the monitoring period (Figs. 4 and A2 in the electronic supplements). The monitoring fluid

491   samples attained calcite saturation at the end of April 2012, about seven weeks after the Phase I

492   injection was terminated, and at end of August, about four weeks after the Phase II injection was

493   terminated, when the fluid pH had increased to >8. In contrast, the monitoring fluid samples

494   were calculated to be supersaturated with respect to siderite shortly after both injections, whereas

495   magnesite was strongly undersaturated during this time (Fig. 5a). Magnesite and siderite were

496   not identified at the Hellisheidi site prior to the injections, but both minerals have been identified

497   by XRD-analysis of drill-cuttings from the Svartsengi geothermal field in SW-Iceland (Franzson,

498   1983; Richter et al., 1999), which has a significantly higher salinity and higher temperature

499   gradient than the CarbFix site. Magnesite-siderite solid solutions were identified in low

500   temperature CO_2 metasomatised basalts in Nuussuaq, West Greenland (Rogers et al., 2006).

501   There calcite appears at a relatively low CO_2 partial pressure, and magnesite-siderite at higher

502   partial pressures (Fig. 6), as predicted by the PHREEQC modelling (Fig. 5a).

503

504   The calculated saturation indices of a number of other carbonate minerals are shown in

505   Figure 5b. Ankerite ($CaFe(CO_3)_2$) is the only carbonate-phase that was supersaturated during the

506   whole monitoring period, that is while Fe^{2+} concentrations are above the detection limit of the

507   spectroscopic method. Ankerite has not been identified in the area. It was however identified

508   during basaltic glass-CO_2 charged water interaction experiments performed at 75°C by Gysi and

509   Stefánsson (2012b), and during basalt, water, supercritical CO_2 interaction experiments reported

510   by McGrail et al. (2006). Similar to calcite, the sampled fluids were calculated to be

511   supersaturated with respect to aragonite ($CaCO_3$) throughout the monitoring period, with the

512   exception of several weeks near the end of, and shortly after both injections (see Fig. 5b).

513   Aragonite was identified by XRD-analysis of drill-cuttings from the area prior to the injections

514   (Alfredsson et al., 2013). Although the fluids were calculated to be supersaturated with respect to

515   dolomite ($CaMg(CO_3)_2$) following both injections, this mineral has not been observed at the

516   CarbFix site. It has been observed however by XRD-analysis as a secondary mineral in drill-

517   cuttings from the saline Svartsengi high-temperature geothermal field in SW-Iceland, as is the

518   case for magnesite and siderite (Franzson, 1983). The calculated saturation indices of three

519   different Ca-Mg-Fe-solid solutions are shown in Figure 5c. All three show similar trends as

520   calcite and aragonite. The $Mg_{0.50}$-$Fe_{0.50}$-CO_3 is the least saturated of the three, but attained

521   saturation after both injections.

522

523   The calculated saturation indices for some sulphur-bearing minerals are shown in Figure
524   5d. The monitoring well fluids were calculated to be undersaturated with respect to native
525   sulphur during the whole monitoring period. In contrast, pyrite (FeS_2), which is one of the most
526   abundant secondary minerals at Hellisheidi at elevated temperature, and was identified at 780 m
527   depth within the HN-02 injection well (Helgadóttir, 2011), was calculated to be supersaturated in
528   all the monitoring fluid samples, showing a slight decrease in its saturation index at the
529   beginning of the Phase II injection and a peak mid-August 2012 concurrent with the first
530   maximum in SF_5CF_3 concentration, indicating the initial breakthrough of the injected Phase II
531   fluids (Fig. 5d). As previously mentioned, calcite was the only crystalline phase identified in the
532   precipitates forming on the pump from well HN-04. Pyrite was, however, identified by XRD-
533   analysis on samples collected from an airlift of the injection well HN-02, confirming formation
534   of pyrite during or after the Phase II injection (Fig. A3 in the electronic supplement). Greigite
535   (Fe_3S4) showed a similar behaviour as pyrite, as this mineral was supersaturated in all
536   monitoring well fluid samples. This mineral was not identified in the area previously, and was
537   not identified by XRD analysis on the airlift samples collected from the injection well HN-02. It
538   is, however, a metastable phase that may be a precursor of pyrite (Deer et al., 1992). Pyrrhotite
539   (Fe_7S_8- FeS) was slightly supersaturated in the fluids sampled during the first weeks of the Phase
540   II injection but undersaturated in all other samples (Fig. 5d). Pyrrhotite was previously identified
541   within the high-temperature system in the Hellisheiði area (e.g. Gunnarsdóttir, 2012), but was
542   not found at the CarbFix site nor identified in XRD analysis on the airlift samples from the
543   injection well HN-02 (Fig. A3 in the electronic supplements). Gunnlaugsson and Arnórsson
544   (1982) reported that below 180°C, geothermal waters in Iceland equilibrate with marcasite
545   (FeS_2) instead of pyrite; marcasite is a pyrite dimorph generally found at lower temperatures
546   (Deer et al., 1992). There was no evidence of marcasite in samples from the CarbFix site, either
547   prior to the injections or in the XRD-analysis from the airlift pumping of well HN-02 (Fig. A3 in
548   the electronic supplement). Mackinawite (($Fe,Ni)_9S_8$) became supersaturated in the fluids
549   sampled at the beginning of the Phase II injection, during the initial breakthrough of the injected
550   Phase II fluid, and it is near to saturation in some monitoring samples collected from October to
551   April 2013 (Fig. 5d). Mackinawite was not been identified in the area, and was not detected by
552   XRD-analysis on the airlift samples from HN-02 (Fig. A3 in the electronic supplement).

553 However, mackinawite typically forms as a nanocrystalline material, whose broad peaks in XRD
554 would be complicated to identify.

555

Saturation indices for other minerals

557 Saturation indices for other selected minerals are shown in Figure 7. Chalcedony (SiO_2)
558 was slightly undersaturated in the monitoring fluid samples prior to the injections, but becomes
559 saturated during Phase I; it then remains saturated for the rest of the monitoring period (Fig. 7a).
560 Chalcedony is a common secondary mineral in the area (e.g. Alfredsson et al., 2013)

561

562 The mineral saturation states for those zeolites that are common in the area are shown in
563 Figure 7b. Analcime, a common Na-zeolite found as an alteration phase at the CarbFix site, was
564 undersaturated in the sampled fluids until about two months after the beginning of the Phase II
565 injection, and then it is subsequently saturated (Fig. 7b). The samples were supersaturated with
566 respect to other zeolites previously found in the area; and the general trend was a decrease in the
567 monitoring fluid saturation index during the Phase I injection with an increase 6-8 weeks after
568 Phase I was started. A slight dip was observed during the Phase II injection and an increase was
569 observed during the second breakthrough of the injected fluid from Phase I (Fig. 7b).

570

571 The mineral saturation states for common clay minerals are shown in Figure 7c. Kaolinite
572 ($Al_2Si_2O_5OH_4$) remained strongly supersaturated in the fluids sampled during the entire
573 monitoring period (Fig. 7c), but increasingly so when the samples had a pH <8, during the
574 injections and in the first weeks thereafter. Kaolinite was identified as a surface alteration
575 product in geothermal areas (e.g. Markússon and Stefánsson, 2011) but has not been identified in
576 subsurface samples collected from wells at Hellisheidi. The saturation state of gibbsite ($Al(OH)_3$)
577 is depicted with the clay minerals; its behaviour was similar to kaolinite, except that it was
578 undersaturated prior to the injections and became saturated when pH dropped below 8 during
579 Phase I. It remained slightly supersaturated during the rest of the monitoring period (Fig. 7c).
580 The saturation states of two other members of the kaolinite group; imogolite ($Al_2SiO_3OH_4$) and
581 allophane ($Al_2O_3SiO_2*H_2O$), were also calculated. Imogolite was undersaturated prior to the
582 injections but became strongly supersaturated during Phase I when the pH drops below 8, and
583 remained supersaturated for the rest of the monitoring period, but decreasingly so as the pH

584   increased (Fig. 7c). Allophane was undersaturated during the whole monitoring period. Smectite

585   was supersaturated in all samples except for the samples taken during, and shortly after the two

586   injections while the pH was <8 (Fig. 7c). Smectite is one of the most abundant secondary

587   minerals in basaltic rocks and has been identified in all wells drilled at Hellisheidi (e.g.

588   Schiffman and Fridleifsson, 1991).

589

Discussion

591   Concentrations for the major elements Ca, Mg, Si, Na, K and Cl and the trace elements

592   Fe and Al calculated using equations (1) and (2), based on the assumption of non-reactive

593   conservative fluid mixing, are shown in Figure 3 together with their corresponding measured

594   concentrations. Corresponding plots for the injected constituents are shown in Figure 2.

595   Measured concentrations, greater than those calculated based on conservative fluid mixing,

596   suggest net dissolution, lower concentrations suggest net precipitation (i.e. "fixation"). Measured

597   Ca, Mg, and Fe concentrations were much higher during the injections and the subsequent days

598   and weeks than that calculated assuming non-reactive conservative mixing. This indicates a net-

599   input of these elements to the fluid consistent with the dissolution of the basalt originally present

600   in the reservoir. The measured concentrations of these elements eventually became lower, and in

601   the case of Mg, measured concentrations became lower than that calculated from non-reactive

602   mechanical mixing (Fig. 3b) about 300 days after the start of the Phase 1 injection, suggesting

603   net-precipitation into secondary minerals after these times.

604

605   Measured and calculated non-reactive conservative mixing concentrations of Si were

606   approximately identical during the first breakthrough of Phase I, but the measured concentrations

607   were lower during the second breakthrough (Fig. 3d). Measured Na and K concentrations were

608   higher than the calculated from non-reactive conservative mixing, with a continuous increase up

609   until the second breakthrough of Phase I, indicating net-release of these elements from the rock

610   to the fluid (Fig. 3e-f). Na and K are the most mobile major elements during the weathering and

611   low temperature alteration of basaltic rocks (Alfredsson et al., 2013; Eiriksdottir et al., 2015;

612   Gislason et al., 1996). Measured Al concentrations were much lower during Phase I than

613   corresponding calculated non-reactive conservative mixing concentrations indicating net Al

614   precipitation during the injection and during the following weeks, while the pH of the samples

615 from well HN-04 was below 8 (Fig. 3g). Subsequently, the measured Al concentration rises

616 slowly, with a small drop during the Phase II injection. From about 300 days after the start of the

617 Phase I injection, and throughout the sampling period, the measured Al concentration in the

618 samples exceeded the corresponding calculated concentrations, indicating a net release of this

619 element from the rocks. Chlorine is a trace element in basaltic rocks (Sigvaldason and

620 Oskarsson, 1976), but is sparingly taken up by secondary minerals, providing an example of a

621 mobile element that behaves conservatively during mechanical mixing and moderate water rock

622 interactions (Arnórsson and Andrésdóttir, 1995; Gislason and Eugster, 1987; Olsson et al.,

623 2014). Measured and calculated conservative mixing concentrations of Cl were approximately

624 identical, except during the second breakthrough of Phase I, when the measured concentrations

625 were slightly lower than the calculated values (Fig. 3h) suggesting its possible uptake into

626 carbonates (Olsson et al., 2014).

627

628 **The fate of the injected carbon**

629   The results and calculations presented above provide insight into the fate of the injected

630 dissolved CO_2 gas. As previously reported by Matter et al. (2016), the difference between the

631 measured and calculated non-reactive mixing DIC concentration (Fig. 8a), indicates its loss

632 along the flow-path towards the monitoring well. Matter et al. (2016) also suggest that the

633 dissolution of pre-existing carbonates at the onset of the CO_2 injection may have contributed to

634 the neutralisation of the injected CO_2-rich water, along with dissolution of other phases such as

635 basaltic glass, primary minerals of the host rock and other secondary minerals. This liberation of

636 cations and neutralization of the originally acidic gas-rich injected aqueous fluid lead to the

637 precipitation of carbonate minerals; Matter et al. (2016) concluded that over 95% of the carbon

638 injected during Phase I was fixed as carbonate minerals in less than two years.

639

640   These previous conclusions are supported by the observations reported in this study.

641 Shortly after the injections, the measured concentrations of dissolved Mg, Fe, and Ca increased

642 substantially (Fig. 3a-c), and were greatly above that computed for non-reactive mixing,

643 consistent with the rapid dissolution of the original reservoir rock. The dissolved concentration

644 of Ca in these fluids was far greater than that of Mg and Fe, suggesting the preferential

645 dissolution of calcium bearing minerals, such as calcite, during and shortly after both injection

646 phases. Indeed, the saturation state of calcite, the major carbonate phase present in the basaltic
647 reservoir became undersaturated during and just after the Phase I injection (Fig .5a), consistent
648 with the initial dissolution of the calcite originally present in the host rock. Approximately 100
649 days after the start of the Phase I injection the monitoring fluid samples became supersaturated
650 with respect to calcite with a saturation index of 0.6; this degree of supersaturation would be
651 sufficient to grow calcite on the surfaces of the silicate minerals present in the reservoir
652 (Stockmann et al., 2014). A similar variation of the calcite saturation state was evident following
653 the Phase II injection. Moreover, calcite was observed to have precipitated within the monitoring
654 well following the injection.

655

656   The saturation state of the monitoring fluid samples with respect to the carbonate phases
657 magnesite and dolomite followed a similar pattern as calcite (Fig. 5b), but these were not
658 identified in the study area. Such minerals have been reported to be kinetically inhibited from
659 forming abiotically at temperatures less than 80 °C (Higgins and Hu, 2005; Kessels et al., 2000;
660 Lippmann, 1973; Saldi et al., 2009, 2012). Similarly, siderite was calculated to be supersaturated
661 in the sampled fluid but has not been found at the study site to date.

662

The fate of the injected sulphur

664   A noteworthy observation in this study is that the dissolved sulphur concentrations in the
665 monitoring well samples remained close to constant during and after the injection of the H_2S-rich
666 phase II injection. In contrast, non-reactive mixing calculations suggest these concentrations
667 should have been as high as 0.6 mmol/L in the absence of sulphur precipitation (Fig. 8b). This
668 indicates that vast majority of the sulphur injected into the subsurface was fixed within several
669 weeks, before the Phase II fluids arrived at the first monitoring well. Indeed, numerous sulphur-
670 bearing minerals, including pyrite, pyrrhotite, mackinawite, and greigite were supersaturated
671 during the first weeks of Phase II injection (Fig. 5d).

672

673   Pyrite was strongly supersaturated favouring its nucleation and subsequent precipitation.
674 The pyrite formation was confirmed by XRD-analysis on solids collected from the water samples
675 taken during airlift from the injection well HN-02 in the spring of 2013. The analysis showed
676 peaks from pyrite, amounting to 5-10 weight% of the solid material present in the air-lift

677 samples, based on Rietveld analysis using the software Topas (Fig. A3 in the electronic

678 supplement). No other well-crystalline sulphides were identified in these airlift samples.

679 Moreover, sulphide minerals were not identified in the precipitates recovered from the HN-04

680 monitoring well pump, which supports the conclusion that the H_2S mineralises prior to the

681 arrival of the injection fluid at the first monitoring well. This rapid mineralisation of the injected

682 H_2S is also in agreement with experimental studies on H_2S sequestration in basaltic rocks

683 (Gudbrandsson and Stefánsson, 2014).

684

685 **The timescale of carbon and sulphur mineralisation: Carbon storage in**

686 **sedimentary basins versus basaltic rocks.**

687 Carbon storage in sedimentary basins typically proceeds via the injection of pure CO_2

688 into porous sedimentary rocks (Fig. 9a). For common geothermal gradients, CO_2 is a

689 supercritical fluid below 800 m in sedimentary basins. As supercritical CO_2 is less dense than the

690 formation waters near this depth, it is buoyant and tends to rise to the surface. Ideally this CO_2 is

691 trapped below an impermeable cap rock via structural or stratigraphic trapping. Eventually some

692 of this CO_2 becomes stuck in small pores, limiting its mobility (residual trapping). Over time,

693 CO_2 dissolves in the formation water (solubility trapping). As CO_2 charged water is denser than

694 the original formation water, this CO_2-charged water will tend to sink. Some of this dissolved

695 CO_2 may react to form stable carbonate minerals (mineral trapping). As one progresses from

696 structural to mineral trapping, the CO_2 becomes more immobile and thus the storage more

697 secure, though this process can take thousands of years or more as summarized in Figure 9a

698 (Benson and Cole, 2008; Benson et al., 2005). Mineral trapping in sedimentary basins is slow

699 and sometimes limited because of a lack of the calcium, magnesium, and iron bearing minerals

700 required to mineralise the injected CO_2 (Gilfillan et al., 2009; Gislason and Oelkers, 2014).

701

702 In contrast during the CarbFix method, CO_2 is dissolved into water during its injection

703 into porous basaltic rocks. No cap rock is required because the dissolved CO_2 is not buoyant and

704 will not tend to migrate back to the surface. Solubility trapping occurs within 5 minutes during

705 the CO_2 injection process (Sigfusson et al., 2015), and due to the reactivity of the basaltic rocks

706 the bulk of the carbon is trapped in minerals within two years as shown in Figure 9b (this study;

707 Matter et al., 2016). This rapid carbonation of injected CO_2 provides a permanent and safe

708   carbon storage option; once fixed into a carbonate mineral, the risk of leakage is minimal and

709   little if any further monitoring of the site will be necessary.

710

711   The results of this study suggest that the co-injection of H_2S with CO_2 into the subsurface both

712   rapidly fixes this gas through pyrite precipitation and does not detrimentally effect the

713   carbonation of the injected CO_2. Indeed, the results from this study indicate that this pyrite

714   mineralization is even faster than the carbonate mineralization; the bulk of the sulphur is trapped

715   in minerals within four months from injection. The co-injection of these two acid gases may

716   provide a number of advantages, most notably, it may lower substantially the energy and cost

717   required to capture and separate the CO_2 from industrial exhaust. This possibility is now being

718   explored in the SulFix-CarbFix project , where a CO_2-H_2S gas mixture is being captured and

719   separated from the gas stream of the Hellisheidi power plant by its dissolution in water at the

720   surface at about 5 bars pressure and 20°C. The resulting gas charged water is directly injected to

721   700 m depth and 200 - 270°, aiming to store 8,000 - 10,000 tonnes of the gas mixture annually.

722

723   The degree to which the CarbFix method can be applied at other sites will depend on the

724   availability of suitable host-rocks, sufficient water to dissolve the CO_2 during its injection, and

725   economic considerations. This on-shore CarbFix project, demonstrates the feasibility of carbon

726   storage in basaltic rocks. Nevertheless, the largest geological storage potential for CO_2 lies

727   offshore (Goldberg and Slagle, 2009; Goldberg et al., 2010; Goldberg et al., 2008;

728   Snæbjörnsdóttir et al., 2014), where the mid-oceanic ridges contain permeable basaltic layers and

729   the oceans provide an unlimited reservoir for the required water (Snæbjörnsdóttir and Gislason,

730   2016).

731

732   **Conclusions**

733   This paper reported the chemical composition and mineral saturation states of fluids

734   collected prior to, during and after the injection of 175 tonnes of pure CO_2 and 73 tonnes of a

735   gas-mixture consisting of 75 mol% CO_2, 24 mol% H_2S and 1 mol% H_2, into basaltic rocks at the

736   CarbFix site in SW-Iceland. All results indicate that the vast majority of injected CO_2 and H_2S

737   were rapidly fixed within minerals in subsurface basalts. The results presented above confirm

738   that this fixation occurred by the initial dissolution of the host basalts due to the injection of

acidic gas-charged water; mass balance indicates the net input from host rock dissolution of Mg, Fe, and Ca following each injection. The dissolution of host basalts and fluid mixing neutralized the pH of the injected fluid such that calcite became supersaturated approximately 100 days after the start of each injection favouring the fixation of the injected CO_2 within this mineral. This results, which supports those of Matter et al. (2016) who concluded that CO_2 mineralization fixed over 95% of the injected carbon within 2 years, was further validated by observations of calcite precipitation within the monitoring well itself. Although other metal carbonate minerals, notably, ankerite, siderite and mixed Ca, Mg, Fe-carbonates, were also supersatutated in the monitoring fluids these were not observed to form during this study.

Similar results support the even more rapid mineralization of injected H_2S as pyrite, as this mineral is supersaturated before, during and after the injection of a mixed CO_2-H_2S charged water into the basalts. The rapid fixation of H_2S into this mineral is further evidenced by the observation of pyrite precipitation in the injection well but not in the first monitoring well. Such observations suggest that H_2S fixation by pyrite precipitation was essentially complete before the injected mixed-gas plume arrived at the monitoring well. Notably there appears to have been little difference in the chemical response in the subsurface of the mixed H_2S-CO_2 gas mixture injection compared to that of the pure CO_2 injection. Their similar success towards the CO_2 mineralization suggests that the injection of mixed gases might prove to be a simpler and more cost-effective approach to subsurface carbon storage than the injection of pure CO_2.

References

Alfredsson, H. A., Oelkers, E. H., Hardarsson, B. S., Franzson, H., Gunnlaugsson, E., and Gislason, S. R., 2013. The geology and water chemistry of the Hellisheidi, SW-Iceland carbon storage site: International Journal of Greenhouse Gas Control, v. 12, p. 399-418.

Aradóttir, E. S. P., Gunnarsson, I., Sigfússon, B., Gislason, S. R., Oelkers, E. H., Stute, M., Matter, J. M., Snæbjörnsdóttir, S. Ó., Mesfin, K. G., Alfredsson, H. A., Hall, J., Arnarsson, M. T., Dideriksen, K., Júlíusson, B. M., Broecker, W. S., and Gunnlaugsson, E., 2015. Towards Cleaner Geothermal Energy: Subsurface Sequestration of Sour Gas Emissions from Geothermal Power Plants, Proceedings World Geothermal Congress 2015: Melbourne, Australia, 19-25 April 2015.

Aradóttir, E. S. P., Sonnenthal, E. L., Björnsson, G., and Jónsson, H., 2012. Multidimensional reactive transport modeling of CO_2 mineral sequestration in basalts at the Hellisheidi geothermal field, Iceland: International Journal of Greenhouse Gas Control, v. 9, p. 24-40.

Archer, D., 2005. Fate of fossil fuel CO_2 in geologic time: Journal of Geophysical Research, v. 110, p. C09S05.

Arnórsson, S., and Andrésdóttir, A., 1995. Processes controlling the distribution of boron and chlorine in natural waters in Iceland: Geochimica et Cosmochimica Acta, v. 59, no. 20, p. 4125-4146.

Arnórsson, S., D'Amore, F., and Gerardo-Abaya, J., 2000. Isotopic and geochemical techniques in geothermal exploration, development and use: Sampling methods, data handling, interpretation. Arnórsson, S. (Ed.), International Atomic Energy Agency Publication, Vienna.

Assayag, N., Matter, J., Ader, M., Goldberg, D., and Agrinier, P., 2009. Water–rock interactions during a CO_2 injection field-test: Implications on host rock dissolution and alteration effects: Chemical Geology, v. 265, no. 1–2, p. 227-235.

Bachu, S., and Gunter, W. D., 2005. Overview of acid-gas injection operations in Western Canada, *in* Wilson, E. S., Rubin, D. W., Keith, C. F., Gilboy, M., Thambimuthu, T., Morris, J., and Gale, K., eds., Greenhouse Gas Control Technologies 7: Oxford, Elsevier Science Ltd, p. 443-448.

Bacon, D. H., Ramanathan, R., Schaef, H. T., and McGrail, B. P., 2014. Simulating geologic co-sequestration of carbon dioxide and hydrogen sulfide in a basalt formation: International Journal of Greenhouse Gas Control, v. 21, p. 165-176.

Benson, S.M. and Cook, P., Coordinating Lead Authors. Anderson, J., Bachu,S., Nimir, H.B., Basu, B., Bradshaw, J., Deguchi, G., Gale, J., von Goerne, G., Heidug, W., Holloway, S., Kamal, R., Keith, D., Lloyd, P., Rocha, P., Senior, B., Thomson, J., Torp, T., Wildenborg, T., Wilson, M., Zarlenga, F., and Zhou, D, Lead Authors. Celia, S.M., Gunter, B., Ennis King, J., Lindegerg, E., Lombardi, S., Oldenburg, C., Pruess, K., Rigg, A., Stevens, S., Wilson, E., Whittaker, S., 2005. Underground Geological Storage, IPCC Special Report on Carbon Dioxide Capture and Storage, Chapter 5. Intergovernmental Panel on Climate Change, Cambridge University Press, Cambridge, U.K.

Benson, S. M., and Cole, D. R., 2008. CO_2 Sequestration in Deep Sedimentary Formations: Elements, v. 4, p. 325-331

Broecker, W., 2007. Climate change: CO_2 arithmetic: Science, v. 315, p. 1371.

Broecker, W. S., and Kunzig, R., 2008. Fixing climate. The story of climate science—and how to stop global warming. Green Profile.

Deer, W. A., Howie, R. A., and Zussman, J., 1992. An introduction to the rock forming minerals. 2nd edition, Harlow, England, Pearson, Prestice Hall, 696 p.

Drever, J. I., 1982. The Geochemistry of Natural Waters, Englewood Cliffs, N. J., Prentice-Hall.

Eiriksdottir, E. S., Gislason, S. R., and Oelkers, E. H., 2015. Direct evidence of the feedback between climate and nutrient, major, and trace element transport to the oceans: Geochimica et Cosmochimica Acta, v. 166, p. 249-266.

European Environment Agency, 2014. Sulphur dioxide (SO_2) emissions (APE 001) - Assessment published in Jan 2014. Volume 2015, European Environment Agency.

828   Fisher, A. T., 1998. Permeability within basaltic oceanic crust: Reviews of Geophysics, v. 36, no. 2, p.
829   143-182.
830   Flaathen, T. K., Gislason, S. R., Oelkers, E. H., and Sveinbjörnsdóttir, Á. E., 2009. Chemical evolution of
831   the Mt. Hekla, Iceland, groundwaters: A natural analogue for CO_2 sequestration in basaltic rocks:
832   Applied Geochemistry, v. 24, no. 3, p. 463-474.
833   Franzson, H., 1983. Svartsengi, well SG-12: Drilling, stratigraphy and aquifers (in Icelandic): National
834   Energy Authority of Iceland, OS/83003/JHD-02.
835   Galeczka, I., Wolff-Boenisch, D., Oelkers, E. H., and Gislason, S. R., 2014. An experimental study of
836   basaltic glass–H_2O–CO_2 interaction at 22 and 50°C: Implications for subsurface storage of CO_2:
837   Geochimica et Cosmochimica Acta, v. 126, p. 123-145.
838   Gensemer, R. W., and Playle, C., 1999, The bioavailability and toxicity of aluminum in aquatic
839   environments: Critical Reviews in Environmental Science and Technology, v. 29, no. 4, p. 315-
840   450.
841   Gilfillan, S. M. V., Lollar, B. S., Holland, G., Blagburn, D., Stevens, S., Schoell, M., Cassidy, M., Ding,
842   Z., Zhou, Z., Lacrampe-Couloume, G., and Ballentine, C. J., 2009. Solubility trapping in
843   formation water as dominant CO_2 sink in natural gas fields: Nature, v. 458, no. 7238, p. 614-618.
844   Gislason, S. R., Arnórsson, S., and Ármannsson, H., 1996. Chemical weathering of basalt in SW Iceland:
845   Effects of runoff, age of rocks and vegetative/glacial cover: American Journal of Science, v. 296,
846   p. 837-907.
847   Gislason, S. R., Broecker, W. S., Gunnlaugsson, E., Snæbjörnsdóttir, S. Ó., Mesfin, K. G., Alfredsson, H.
848   A., Aradottir, E. S., Sigfusson, B., Gunnarsson, I., Stute, M., Matter, J. M., Arnarson, M. T.,
849   Galeczka, I. M., Guðbrandsson, S., Stockman, G., Wolff-Boenisch, D., Stefansson, A.,
850   Ragnheidardottir, E., Faathen, T., Gysi, A. P., Olssen, J., Didriksen, K., Stippe, S., Menez, B.,
851   and Oelkers, E. H., 2014. Rapid solubility and mineral storage of CO_2 in basalt: Energy Procedia,
852   v. 63, p. 4561-4574.
853   Gislason, S. R., and Eugster, H. P., 1987. Meteoric water-basalt interactions. I: A laboratory study:
854   Geochimica et Cosmochimica Acta, v. 51, no. 10, p. 2827-2840.
855   Gislason, S. R., and Oelkers, E. H., 2014. Carbon Storage in Basalt: Science, v. 344, p. 373-374.
856   Gislason, S. R., and Torssander, P., 2006. Response of Sulfate Concentration and Isotope Composition in
857   Icelandic Rivers to the Decline in Global Atmospheric SO_2 emissions into the North Atlantic
858   Region: Environmental Science and Technology, v. 40, p. 680-686.
859   Gislason, S. R., Wolff-Boenisch, D., Stefansson, A., Oelkers, E. H., Gunnlaugsson, E., Sigurdardottir, H.,
860   Sigfusson, B., Broecker, W. S., Matter, J., Stute, M., Axelsson, G., and Fridriksson, T., 2010.
861   Mineral sequestration of carbon dioxide in basalt: A preinjection overview of the CarbFix project:
862   International Journal of Greenhouse Gas Control, v. 4, p. 537-545.
863   Global CCS Institute, 2015. The global Status of CCS 2015 – summary report. Melbourne, Australia.
864   Goldberg, D., Lackner, K., Han, P., and Wang, T., 2013, Co-Location of Air Capture, Subseafloor CO_2
865   Sequestration, and Energy Production on the Kerguelen Plateau: Environmental Science and
866   Technology, v. 47, no. 13.
867   Goldberg, D., and Slagle, A. L., 2009. A global assessment of deep-sea basalt sites for carbon
868   sequestration: Energy Procedia, v. 1, p. 3675-3682.
869   Goldberg, D. S., Kent, D. V., and Olsen, P. E., 2010. Potential on-shore and off-shore reservoirs for CO_2
870   sequestration in Central Atlantic magmatic province basalts: Proceedings of the National
871   Academy of Sciences of the United States of America Sciences, v. 107, p. 1327-1332.
872   Goldberg, D. S., Takahashi, T., and Slagle, A. L., 2008. Carbon dioxdie sequestration in deep-sea basalt:
873   PNAS, v. 105, no. 29, p. 9920-9925.
874   Gudbrandsson, S., and Stefánsson, A., 2014. Experimental study of H_2S sequestration in geothermal
875   systems, RH-14-2014.
876   Gudbrandsson, S., Wolff-Boenisch, D., Gislason, S. R., and Oelkers, E. H., 2011. An experimental study
877   of crystalline basalt dissolution from $2 < pH < 11$ and temperatures from 5 to 75 °C: Geochimica
878   et Cosmochimica Acta, v. 75, no. 19, p. 5496-5509.

879 Gunnarsdóttir, S. H., 2012. The Geology and Hydrothermal Alteration near the Mt. Reykjafell area in the
880   Hellisheidi Geothermal Field. (MSc thesis). University of Iceland.
881 Gunnarsson, I., Sigfusson, B., Stefansson, A., Arnorsson, S., Scott, S., and Gunnlaugsson, E., 2011.
882   Injection of H_2S from Hellisheiði Power Plant, Iceland, Workshop on Geothermal Reservoir
883   Engineering: Stanford, California.
884 Gunnlaugsson, E., and Arnòrsson, S., 1982. The chemistry of iron in geothermal systems in iceland:
885   Journal of Volcanology and Geothermal Research, v. 14, no. 3–4, p. 281-299.
886 Gysi, A. P., and Stefánsson, A., 2011. CO_2–water–basalt interaction. Numerical simulation of low
887   temperature CO_2 sequestration into basalts: Geochimica et Cosmochimica Acta, v. 75, no. 17, p.
888   4728-4751.
889 -, 2012a. CO_2-water–basalt interaction. Low temperature experiments and implications for CO_2
890   sequestration into basalts: Geochimica et Cosmochimica Acta, v. 81, p. 129-152.
891 -, 2012b. Mineralogical aspects of CO_2 sequestration during hydrothermal basalt alteration — An
892   experimental study at 75 to 250°C and elevated pCO_2: Chemical Geology, v. 306–307, p. 146-
893   159.
894 Harris, R. N., and Chapman, D. S., 2004. Deep-seated oceanic heat flux, heat deficits and hydrothermal
895   circulation, Cambridge, Cambridge University Press, Hydrogeology of the Oceanic Lithosphere.
896 Helgadóttir, H. M., 2011, Stratigraphy and hydrothermal alteration of the Gráuhnúkar geothermal system
897   in the southern part of the Hengill area. (MSc Thesis). University of Iceland, 123 p.
898 Higgins, S. R., and Hu, X., 2005. Self-limiting growth on dolomite: Experimental observations with *in*
899   *situ* atomic force microscopy: Geochimica et Cosmochimica Acta, v. 69, p. 2085-2094.
900 Hjartarson, Á., and Sæmundsson, K., 2014. Geological Map of Iceland. Bedrock. 1:600 000: Iceland
901   GeoSurvey.
902 Hoffert, M., Caldeira, K., Benford, G., Criswell, D., Green, C., Herzog, H., Jain, A., Kheshgi, H.,
903   Lackner, K., Lewis, J., Lightfood, H., Manheimer, W., Mankins, J., Mauel, M., Perkins, L.,
904   Schlesinger, M., Volk, T., and Wigley, T., 2002, Advanced technology paths to global climate
905   stability: energy for a greenhouse planet.: Science, v. 298, no. 981-987.
906 International Engy Agency, 2015. Mobilising Innovation to Accelerate Climate Action, Executive
907   Summary.
908 IPCC, 2005. IPCC Special Report on Carbon Dioxide Capture and Storage. Prepared by
909   Working Group III of the Intergovernmental Panel on Climate Change . Metz, B.,
910   Davidson, O., de Coninck, H.C., Loos, M., and Meyer, L. A. (eds.). Cambridge University
911   Press, Cambridge, United Kingdom and New York, NY, USA, 442 pp.
912 -, 2014. Contribution of Working Groups I, II and III to the Fifth Assessment Report of the
913   Intergovernmental Panel on Climate Change.
914 Kessels, L. A., Sibley, D. F., and Nordeng, S. H., 2000. Nanotopography of synthetic and natural
915   dolomite crystals.: Sedimentology, v. 47, p. 173-186.
916 Khalilabad, M. R., Axelsson, G., and Gislason, S. R., 2008. Aquifer characterization with tracer test
917   technique; permanent CO_2 sequestration into basalt, SW Iceland: Mineralogical Magazine, v. 72,
918   p. 121-125.
919 Knauss, K.G., Johnson, J.W., Steefel, C.I., 2005. Evaluation of the impact of CO_2, co-contaminant gas,
920   aqueous fluid and reservoir rock interactions on the geologic sequestration of CO_2. Chemical
921   Geology, v. 217, no. 3–4, p. 339–350.
922 Lackner, K., 2003. A guide to CO_2 sequestration.: Science v. 300, p. 1677–1678.
923 Lippmann, F., 1973. Sedimentary carbonate minerals., New York, Springer-Verlag.
924 Markússon, S. H., and Stefánsson, A., 2011. Geothermal surface alteration of basalts, Krýsuvík Iceland—
925   Alteration mineralogy, water chemistry and the effects of acid supply on the alteration process:
926   Journal of Volcanology and Geothermal Research, v. 206, no. 1–2, p. 46-59.
927 Matter, J., Takahashi, T., and Goldberg, D., 2007. Experimental evaluation of *in situ* CO_2-water-rock
928   reactions during CO_2 injection in basaltic rocks: Implications for geological CO_2 sequestration:
929   Geochem Geophy Geosy 6, v. 8, no. 2, p. 19.

930   Matter, J. M., Broecker, W., Gislason, S. R., Gunnlaugsson, E., Oelkers, E., Stute, M., Sigurdardóttir, H.,
931   Stefansson, A., Wolff-Boenisch, D., Axelsson, G., and Sigfússon, B., 2011. The CarbFix Pilot
932   Project - Storing Carbon Dioxide in Basalt: Energy Procedia v. 4, p. 5579-5585.
933   Matter, J. M., Stute, M., Snæbjörnsdóttir, S. Ó., Oelkers, E. H., Gislason, S. R., Aradottir, E. S.,
934   Sigfusson, B., Gunnarsson, I., Sigurdardottir, H., Gunnlaugsson, E., Axelsson, G., Alfredsson, H.
935   A., Wolff-Boenisch, D., Mesfin, K., Fernandez de la Reguera Taya, D., Hall, J., Dideriksen, K.,
936   and Broecker, W. S., 2016. Rapid carbon mineralisation for permanent and safe disposal of
937   anthropogenic carbon dioxide emissions: Science. Accepted.
938   McGrail, B. P., Freeman, C. J., Brown, C. F., Sullivan, E. C., White, S. K., Reddy, S., Garber, R. D.,
939   Tobin, D., Gilmartin, J. J., and Steffensen, E. J., 2012. Overcoming business model uncertainty in
940   a carbon dioxide capture and sequestration project: Case study at the Boise White Paper Mill:
941   International Journal of Greenhouse Gas Control, v. 9, p. 91-102.
942   McGrail, B. P., Schaef, H. T., Ho, A. M., Chien, Y.-J., Dooley, J. J., and Davidson, C. L., 2006. Potential
943   for carbon dioxide sequestration in flood basalts: Journal of Geophysical Research v. Solid Earth
944   (111), no. B12201.
945   McGrail, B. P., Spane, F. A., Sullivan, E. C., Bacon, D. H., and Hund, G., 2011. The Wallula basalt
946   sequestration pilot project: Energy Procedia, v. 4, p. 5653-5660.
947   Oelkers, E., and Schott, J., 2005. Geochemical aspects of CO_2 sequestration.: Chemical Geology, v. 217,
948   p. 183–186.
949   Oelkers, E. H., and Cole, D. R., 2008. Carbon dioxide sequestration: a solution to a global problem.:
950   Elements, v. 4, p. 305–310.
951   Oelkers, E. H., Gislason, S. R., and Matter, J., 2008. Mineral carbonation of CO_2.: Elements, v. 4, p. 331–
952   335.
953   Olsson, J., Stipp, S. L. S., Makovicky, E., and Gislason, S. R., 2014. Metal scavenging by calcium
954   carbonate at the Eyjafjallajökull volcano: A carbon capture and storage analogue: Chemical
955   Geology, v. 384, p. 135-148.
956   Pacala, S., and Socolow, R., 2004. Stabilization wedges: solving the climate problem for the next 50 years
957   with current technologies: Science, v. 305, no. 968-971.
958   Parkhurst, D. L., and Appelo, C. A. J., 2013. Description of input and examples for PHREEQC version
959   3—A computer program for speciation, batch-reaction, one-dimensional transport, and inverse
960   geochemical calculations, U.S. Geological Survey Techniques and Methods, v. chap. A43, 497 p.
961   Richter, B., Guðlaugsson, S. Þ., Steingrímsson, B., Björnsson, G., Bjarnason, J. Ö., and Þórhallson, S.,
962   1999. Svartsengi well SJ-18: Drilling, research and production (in Icelandic), OS-99117.
963   Rogers, K. L., Neuhoff, P. S., Pedersen, A. K., and Bird, D. K., 2006. CO_2 metasomatism in a basalt-
964   hosted petroleum reservoir, Nuussuaq, West Greenland: Lithos, v. 92, no. 1–2, p. 55-82.
965   Rosenbauer, R. J., Thomas, B., Bischoff, J. L., and Palandri, J., 2012. Carbon sequestration via reaction
966   with basaltic rocks: Geochemical modelling and experimental results: Geochimica et
967   Cosmochimica Acta, v. 89, p. 116−133.
968   Rutqvist, J., Birkholzer, J., Cappa, F., and Tsang, C.-F., 2007. Estimating maximum sustainable injection
969   pressure during geological sequestration of CO_2 using coupled fluid flow and geomechanical
970   fault-slip analysis. : Energy Conversion and Management, v. 48, p. 1798–1807.
971   Saldi, D., Jordan, G., Schott, J., and Oelkers, E. H., 2009. Magnesite growth rates as a function of
972   temperature and saturation state.: Geochim. Cosmochim. Acta v. 73, p. 5646–5657.
973   Saldi, G. D., Schott, J., Pokrovsky, O. S., Gautier, Q., and Oelkers, E. H., 2012. An experimental study of
974   magnesite precipitation rates at neutral to alkaline conditions and 100–200 C as a function of pH,
975   aqueous solution composition and chemical affinity: Geochimica et Cosmochimica Acta, v. 83, p.
976   93-109.
977   Schiffman, P., and Fridleifsson, G. O., 1991. The smectite-chlorite transition in drillhole NJ-15,
978   Nesjavellir Geothermal Field, Iceland: XRD, BSE and electron microprobe investigations:
979   Journal of Metamorphic Geology, v. 9, no. 6, p. 679-696.

980 Sigfusson, B., Gislason, S. R., Matter, J. M., Stute, M., Gunnlaugsson, E., Gunnarsson, I., Aradottir, E. S.,
981   Sigurdardottir, H., Mesfin, K. G., Alfredsson, H. A., Wolff-Boenisch, D., Arnarson, M. T., and
982   Oelkers, E. H., 2015. Solving the carbon-dioxide buoyancy challenge: The design and field
983   testing of a dissolved CO_2 injection system: Int. J. Greenhouse Gas Control, v. 37, p. 213-219.
984 Sigvaldason, G. E., and Oskarsson, N., 1976. Chlorine in basalts from Iceland: Geochim. Cosmochim.
985   Acta, v. 40, p. 777-789.
986 Smith, S. J., Van Aardenne, J., Klimont, Z., Anders, R. J., Volke, A., and Delgato Arias, S., 2011.
987   Anthropogenic sulfur dioxide emissions 1850-2005: Amospheric Chemistry and Physics, v. 11, p.
988   1101-1116.
989 Snæbjörnsdóttir, S. Ó., and Gislason, S. R., 2016. CO_2 storage potential of basaltic rocks offshore Iceland:
990   Energy Procedia, v. 86, p. 371-380.
991 Snæbjörnsdóttir, S. Ó., Wiese, F., Fridriksson, T., Ármannsson, H., Einarsson, G. M., and Gislason, S. R.,
992   2014. CO_2 storage potential of basaltic rocks in Iceland and the oceanic ridges: Energy Procedia,
993   v. 63, p. 4585-4600.
994 Stefánsson, A., Arnórsson, S., Gunnarsson, I., Kaasalainen, H., and Gunnlaugsson, E., 2011. The
995   geochemistry and sequestration of H_2S into the geothermal system at Hellisheidi, Iceland: Journal
996   of Volcanology and Geothermal Research, v. 202, no. 3–4, p. 179-188.
997 Stockmann, G. J., Wolff-Boenisch, D., Bovet, N., Gislason, S. R., and Oelkers, E. H., 2014. The role of
998   silicate surfaces on calcite precipitation kinetics: Geochimica et Cosmochimica Acta, v. 135, p.
999   231-250.
1000 Stockmann, G. J., Wolff-Boenisch, D., Gislason, S. R., and Oelkers, E. H., 2011. Do carbonate
1001   precipitates affect dissolution kinetics? 1: Basaltic glass: Chemical Geology, v. 284, no. 3–4, p.
1002   306-316.
1003 Stockmann, G. J., Wolff-Boenisch, D., Gislason, S. R., and Oelkers, E. H., 2013. Do carbonate
1004   precipitates affect dissolution kinetics?: 2: Diopside: Chemical Geology, v. 337–338, p. 56-66.
1005 Stumm, W., and Morgan, J. J., 1996. Aquatic Chemistry: Chemical equilibria and rates in natural waters
1006   (third ed.), John Wiley & Sons, New York, 1022 p.:
1007 Thorarinsson, S. B., Helgadóttir, H. M., Franzson, H., Harðarson, B. S., Hjartarson, A., Ásmundsson, R.,
1008   and Sigurdsson, G., 2006. Hellisheidi - well HN-04. 1st to 3rd stages: Drilling of 18 5/8" security
1009   casing in 105 m, production casing in 400 m and 12 1/4" production part in 1204 m: ISOR,
1010   Iceland GeoSurvey, ISOR-2006/055.
1011 United States Environmental Protection Agency, 2015. The National Emissions Inventory. National
1012   Summary of Sulfur Dioxide Emissions, NEI 2011 v2 GPR.
1013 Van Pham, H., Aagaard, P., and Hellevang, H., 2012. On the potential for CO_2 mineral storage in
1014   continental flood basalts - PHREEQC batch and 1D diffusion - reaction simulations:
1015   Geochemical Transactions, v. 13, no. 5, p. 12.
1016 Wiese, F., Fridriksson, T., and Armannsson, H., 2008. CO_2 Fixation by Calcite in High-temperature
1017   Geothermal Systems in Iceland: ISOR, Iceland Geosurvey, ISOR−2008/003
1018 Wolff-Boenisch, D., Wenau, S., Gislason, S. R., and Oelkers, E. H., 2011. Dissolution of basalts and
1019   peridotite in seawater, in the presence of ligands, and CO_2: Implications for mineral sequestration
1020   of carbon dioxide: Geochimica et Cosmochimica Acta, v. 75, no. 19, p. 5510-5525.
1021 World Health Organization, 2000. WHO air quality guidelines for Europe, 2nd edition: WHO regional
1022   office for Europe.
1023 WorleyParsons, and Schlumberger, 2011. Assessment of Carbon Capture and Storage Technologies:
1024   2011, update: Global CCS Institute.
1025 Wöll, C., Hallsdóttir, B. S., Guðmundsson, J., Snorrason, A., Þórsson, J., Jónsson, P. V. K., Andrésson,
1026   K., and Einarsson, S., 2014. Emissions of greenhouse gases in Iceland from 1990 to 2012.
1027   National Inventory report 2014.: Environment Agency of Iceland, UST-2014-2.

Tables

Table 1. Characteristics of the two gas injections into the CarbFix storage site considered in this study.

	Phase I: Injection of 100% CO_2	Phase II: Injection of 75% CO_2, 24% H_2S, 1% H_2
Period:	24th of January to 9th March 2012	15th of June to 1st of August 2012
Injection period (days)	45 Active: 40	48 Active: 29
Mass of injected gas (Tonnes)	175	73
Tracers:		
Reactive	^{14}C	^{14}C
Concentration:	40.0 Bq/L*	6 Bq/L*
^{14}C:^{12}C ratio	2.16×10^{-11}*	6.5×10^{-12}*
Non-reactive	SF_6	SF_5CF_3
Concentration:	2.33×10^{-8} ccSTP/cc*	2.24×10^{-8} ccSTP/cc*

From Matter et al. 2016

Table 2. The measured chemical composition of water collected from well HN-01, and co-injected with pure CO_2 gas or CO_2/H_2S gas mixtures into the CarbFix storage site.

Date	Sample ID	pH	Conductivity	H_2S	O_2	Alk.	DIC	$S_{(total)}$
			µs/cm	µmol/L	mmol/L	mmol/L	mmol/L	mmol/L
3.2.2012	12KGM06	9.29	292	0.45	0.051	2.109	1.460	0.118
4.7.2012	12SOS03	9.21	300	0.32*	0.082	2.046	1.550	0.085

Date	Sample ID	pH	Ca	Mg	Fe	Si	Na	K	Al	Cl
			mmol/L	mmol/L	µmol/L	mmol/L	mmol/L	mmol/L	µmol/L	mmol/L
3.2.2012	12KGM06	9.29	0.13	0.16	0.021	0.59	2.04	0.024	1.19	0.31
4.7.2012	12SOS03	9.21	0.15	0.20	0.068	0.39	1.83	0.024	0.65	0.25

*Measured on 12th of July

Table 3. The measured chemical composition of the major elements of two solid samples collected from the water pump recovered from well HN-04 on the 13th of August 2013.

Si mmol/L	Na mmol/L	K mmol/L	Ca mmol/L	Mg mmol/L	S mmol/L	Al mmol/L	Fe mmol/L
185	14.8	1.00	9482	136	10.0	0.03	286.5
171	11.3	0.49	10230	123	5.3	0.02	197.0

Figures
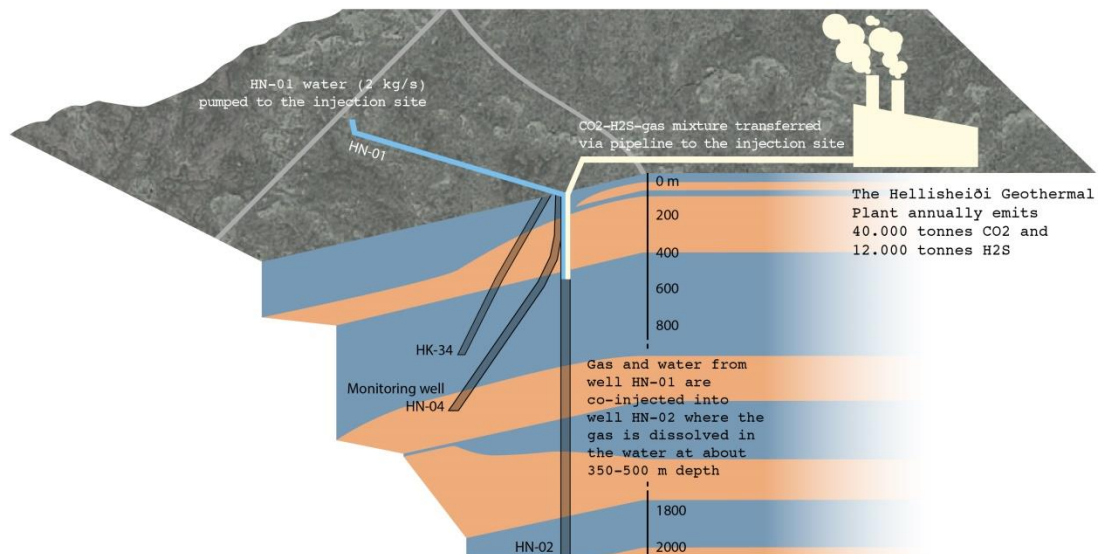
Figure 1. Geological cross section of the CarbFix injection site, modified from Alfredsson et al. (2013). Blue indicates lava flows and brown indicates hyaloclastic (glassy) formations. The CO_2-H_2S-H_2 gas mixture used in the second injection was separated from other geothermal gases at the power plant and transported via gas pipe to the injection site where it was dissolved in water from well HN-01 within the injection well HN-02. The gas charged water enters the basalts as a single phase. Water was pumped from well HN-01 to the injection well HN-02 at the rate of 7.2 m^3/h. Water was pumped from the monitoring well at the rate of 3.5 m^3/h, throughout this study. Graphic work by Sölvi Snæbjörnsson.
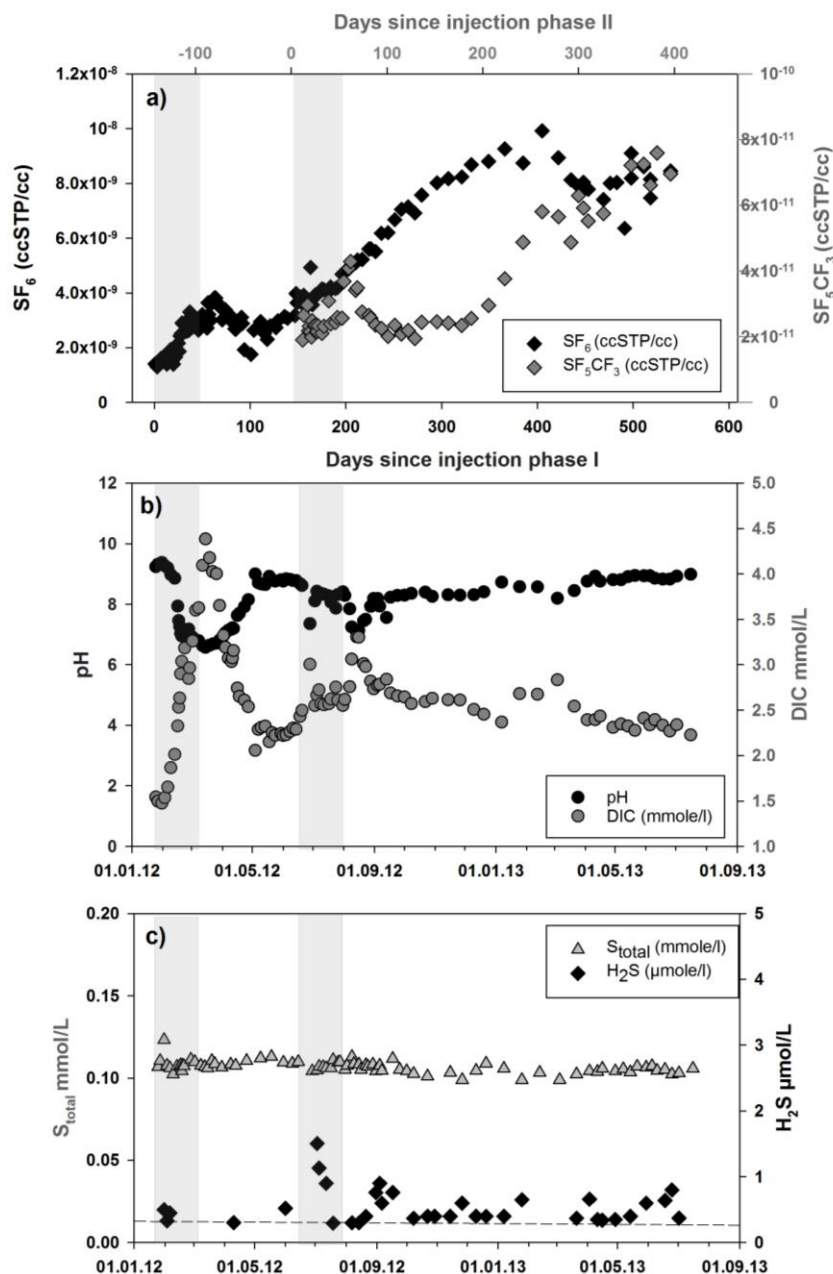
Figure 2. Concentrations of a) SF_6 and SF_5CF_3 non-reactive tracers; b) dissolved inorganic carbon (DIC) along with fluid pH calculated at *in situ* temperature (35°C), c) total dissolved sulphur and $H_2S_{(aq)}$ in samples from monitoring well HN-04 prior to, during, and after the injection of pure CO_2 and mixed CO_2/H_2S gas into the CarbFix Storage site. The timing of both gas injections is indicated by grey bars. The detection limit of the H_2S concentration measurements is 0.3 µmol/L and is indicated as a dotted line.
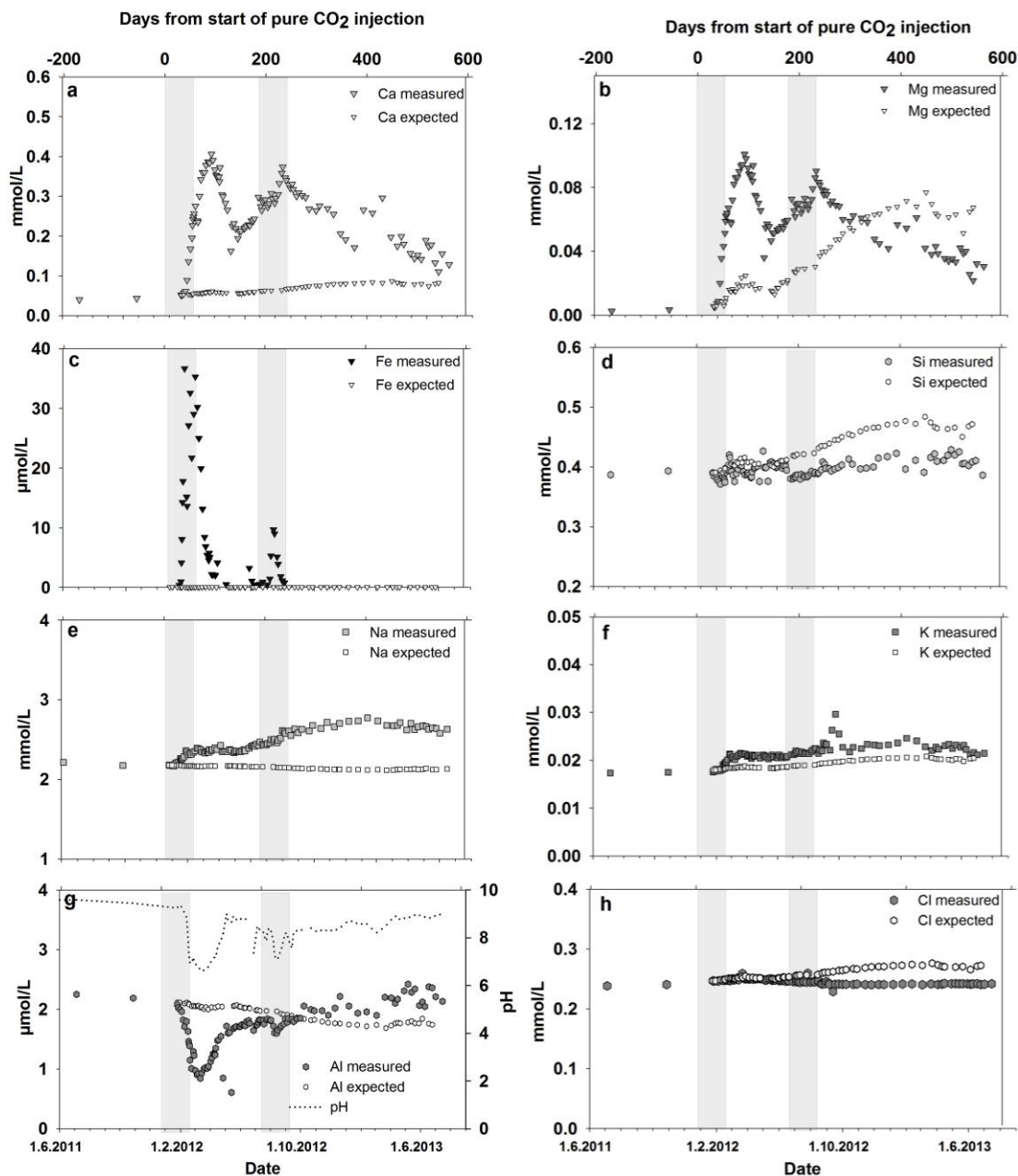
Figure 3. Concentrations of Ca, Mg, Fe, Si, Na, K, Al, Cl and F collected from monitoring well HN-04 prior to, during, and after the injection of CO_2 and CO_2/H_2S into the CarbFix Storage site. The timing of both gas injections is indicated by grey bars. Note the pH of the fluid samples is plotted together with the Al concentrations. The results of mass balance calculations depicting expected values for these concentrations, assuming pure mechanical mixing of the injected solution is also shown in these plots.

Figure 4. Photograph illustrating the presence of precipitates on the water sampling pump recovered from monitoring well HN-04 on the 13th of August 2013. The diameter of the pump is 101 mm.
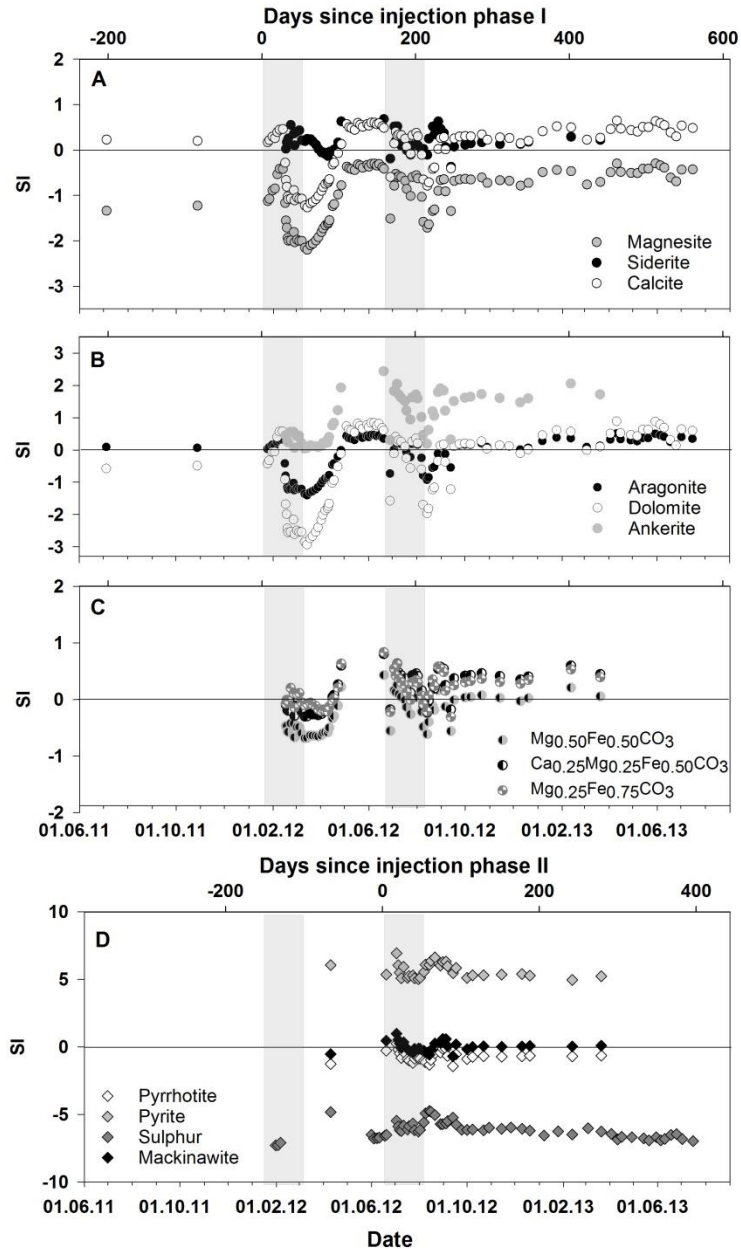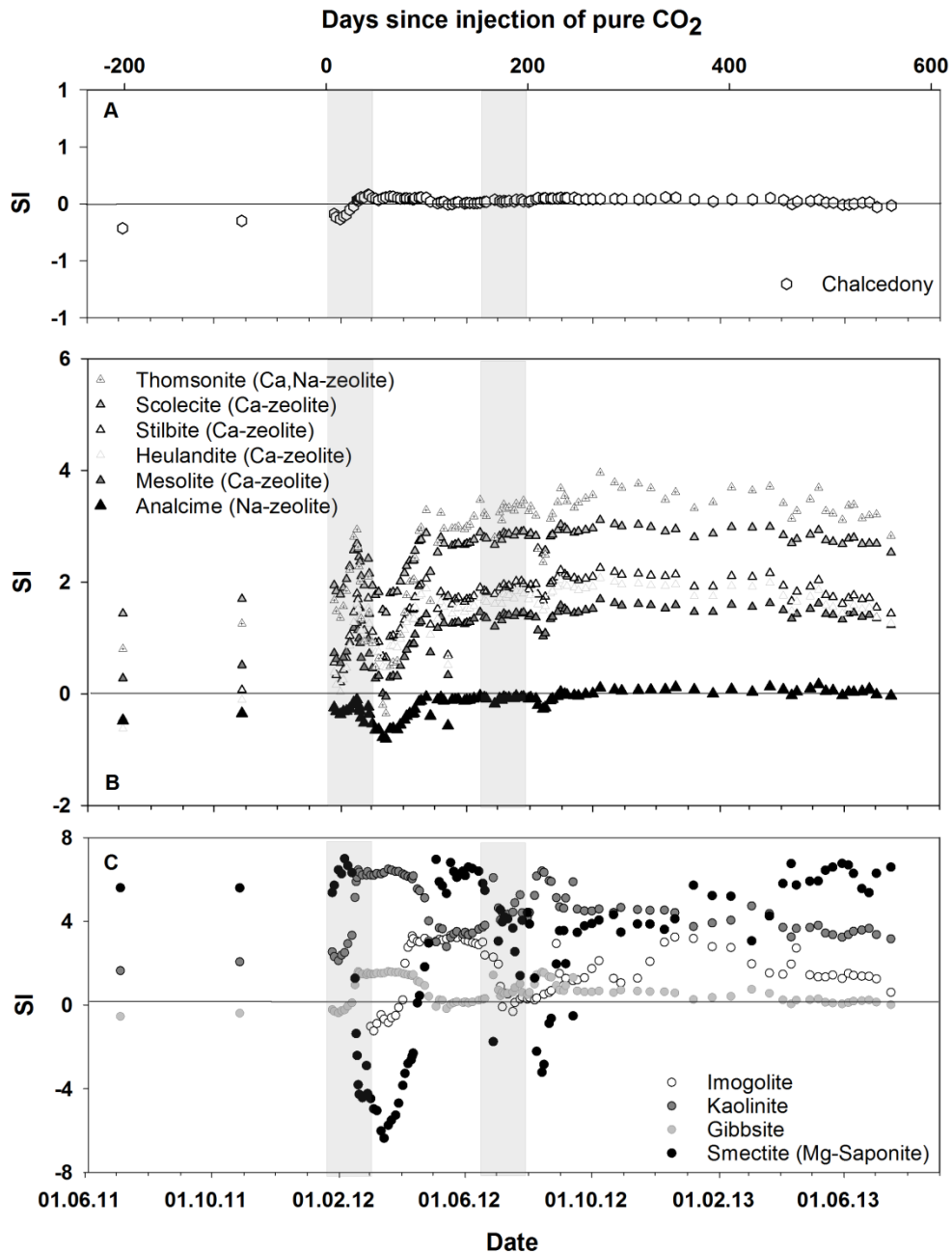
Figure 5. Saturation indices (SI) of collected HN-04 well water samples with respect to A) magnesite siderite and calcite; B) dolomite, aragonite and ankerite, C) Mg-Fe and Ca-Mg-Fe solid solutions, and D) pyrrhotite, pyrite, sulphur and mackinawite prior to, during, and after the injection of pure CO_2 and a CO_2/H_2S gas mixture into the CarbFix Storage site. All saturation indices were calculated assuming the oxygen fugacity was controlled by equilibrium of the H_2S/SO_4^{2-} as a redox couple. Note that positive, negative, and zero SI values correspond to aqueous fluids that are supersaturated, undersaturated, and at equilibrium with the indicated mineral. The timing of both gas injections is indicated by grey bars.
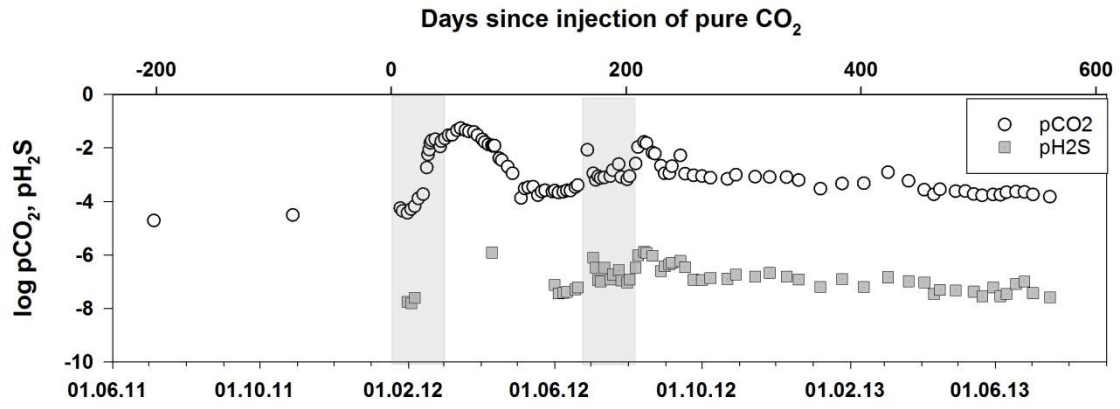
Figure 6. Partial pressures of CO_2 and H_2S prior to, during and after both injection experiments.

Figure 7. Saturation indices (SI) of collected HN-04 well water samples with respect to A) chalcedony, B) the zeolites previously identified in the area, and C) selected clay-minerals prior to, during, and after the injection of pure CO_2 and a CO_2/H_2S gas mixture into the CarbFix Storage site. Note that positive, negative, and zero SI values correspond to aqueous fluids that are supersaturated, undersaturated, and at equilibrium with the indicated mineral. The timing of both gas injections is indicated by grey bars.
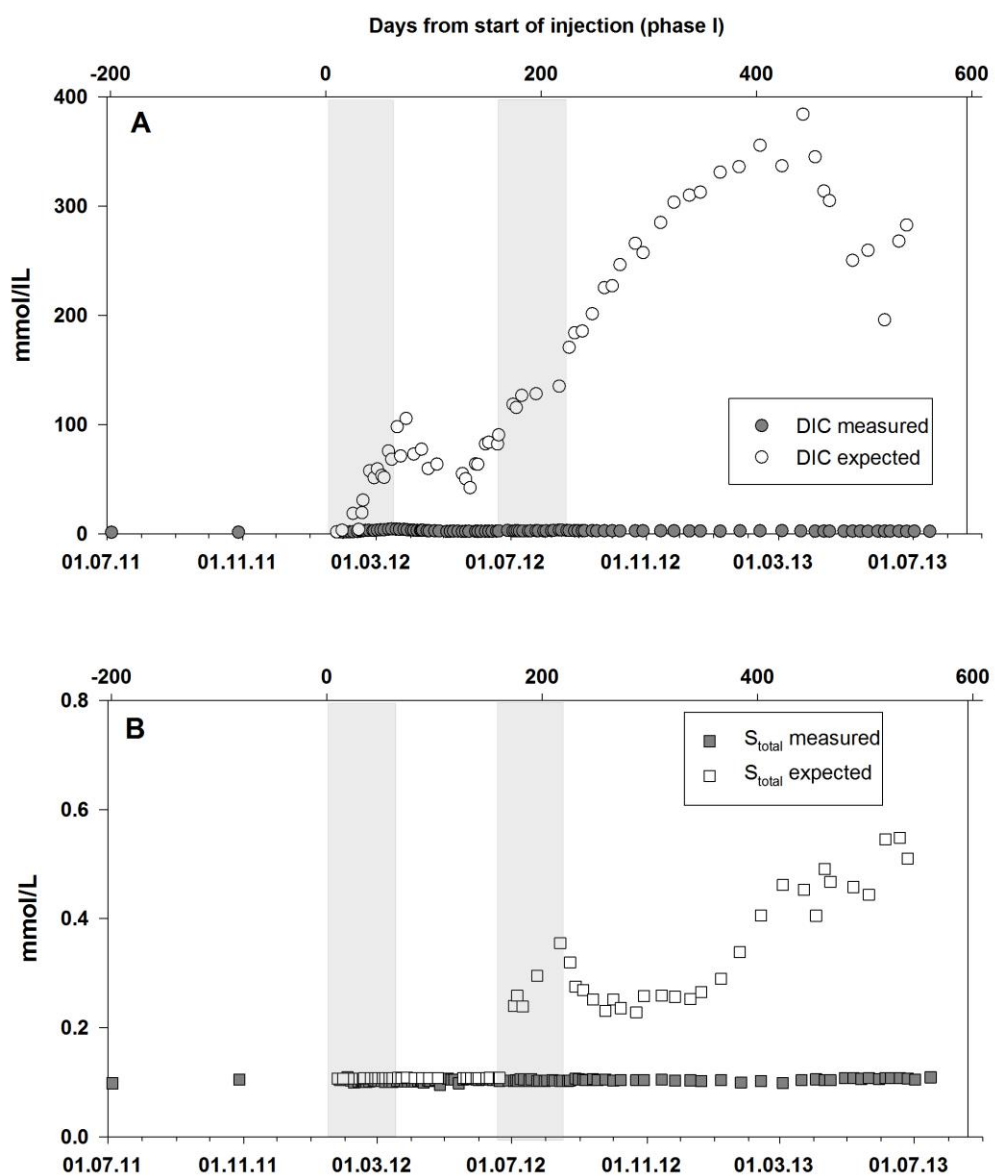
Figure 8. Comparison of measured and calculated non-reactive mixing concentrations of DIC and sulphur – see text. The timing of both gas injections is indicated by grey bars.
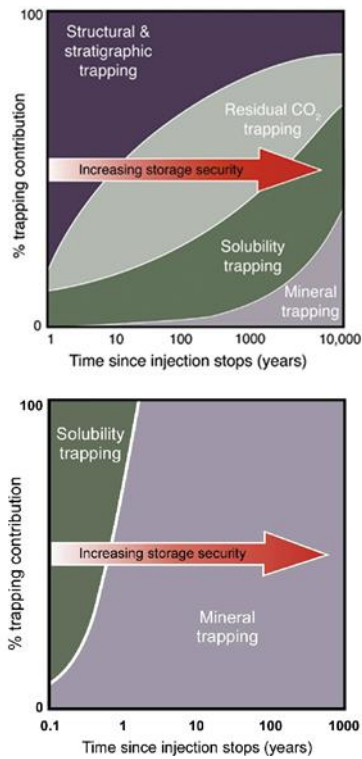
Figure 9. Schematic illustration of the contribution of various trapping mechanisms to the geologic storage as a function of time, a) injection of buoyant supercritical CO_2 into sedimentary rocks, modified from Benson et al. (2005), b) injection of CO_2 dissolved in water into basaltic rocks via the CarbFix method.